

Stability of a two-fluid rod annular flow

S. H. Ferguson Briggs ^{1,*}, M. G. Blyth,² and A. J. Mestel ¹¹*Imperial College London, Exhibition Road, South Kensington, London SW7 2BX, United Kingdom*²*School of Engineering, Mathematics and Physics, University of East Anglia, Research Park, Norwich NR4 7TJ, United Kingdom*

(Received 22 November 2024; accepted 11 February 2025; published 10 March 2025)

Two concentric fluid annuli are enclosed in the gap between an axial rod and an outer cylinder. Motion is driven both by a pressure gradient and by axial translation of the rod. The linear stability of the flow to axisymmetric and nonaxisymmetric disturbances is studied. New stability regions in parameter space are found for both a stationary and a moving rod. If the fluid viscosities differ, the flow can control the capillary instability at the fluid interface, but may itself be unstable, both at moderate Reynolds number and in the inviscid limit. These flow instabilities may be concentrated either at the interface or the solid boundaries. The interplay between these instabilities depends critically on the problem parameters, and nonaxisymmetric modes can be the most unstable. When the outer fluid is more viscous than the inner, complete stabilization can occur for a sufficiently thick stationary rod, whereas in the absence of the rod, the system is always unstable. Moving the rod can have a stabilizing influence either with or without the driving pressure gradient.

DOI: [10.1103/PhysRevFluids.10.034001](https://doi.org/10.1103/PhysRevFluids.10.034001)

I. INTRODUCTION

Core-annular flow (CAF) arises when two fluids of different viscosities arranged in concentric annuli are driven through a cylindrical pipe by an axial pressure gradient. Introducing a rod down the axis of the configuration transforms the system into a rod annular flow (RAF). These flows have numerous applications; for example, CAF is important in the understanding of fluid transportation, oil extraction, and respiratory airflow dynamics, while RAF models well the surgical technique of thread injection for medical implants [1] and coating technology [2]. In the latter, the moving wire acts as a guide for a double coating of die or substrate, and the stability of the two-fluid flow is crucial for a smooth and accurate application. The stability of RAF is nontrivially governed by capillary action and shear stresses at the interface, as well as the presence of the rod and outer wall. It is well known that a cylindrical column of fluid is unstable as a result of capillary forcing if the wavelength of the perturbation is greater than the circumference of the undisturbed interface [3]. The seminal analysis for an inviscid fluid column surrounded by a vacuum has since been extended both linearly and nonlinearly in viscous settings by many authors (for example, Refs. [4–6]). The numerous studies show that in a stationary system, the stability condition remains the same when the fluid column is surrounded by another fluid of different viscosity, and when the system is enclosed by an outer wall. Moreover, Ref. [7] found the stability condition holds when a thin viscous liquid layer coats a rod in both the inviscid and Stokes limits.

*Contact author: sf218@ic.ac.uk

When the fluids are set in nonuniform motion, the dynamics and stability are significantly altered. A shearing force acts at the interface, working to move the fluid with higher viscosity toward the region of stronger shear [8–10]. Reference [11] investigated two-fluid plane Poiseuille flow with a long-wave approximation, demonstrating that viscous stratification can be destabilizing, to an extent determined by the depth ratio of the two fluids. Reference [12] solved the same system numerically for arbitrary wavelength, identifying the different possible instability mechanisms. When viscous effects at the interface dominate, interfacial modes may be destabilized, but the presence of the boundary walls can stabilize the flow. However, under certain parameter regimes, viscous effects at the boundary walls are critical, and an instability develops related to shear modes in single-fluid plane Poiseuille flow. Reference [18] shows that Reynolds stress drives the unstable shear modes, while the interfacial modes rely on energy transfer via the tangential stress at the interface. Interestingly, the unstable shear mode requires a thin layer of less viscous fluid at the wall, and it is in this layer that the Reynolds stress is high.

For a CAF, Ref. [13] showed experimentally that, irrespective of the initial arrangement of fluids, the high-viscosity liquid will always end up occupying the central location in the absence of gravity. Reference [10] explains this using a variational criterion, illustrating how the forcing works to maximize the mass flux by arranging the fluids such that the extremal solution has the high-viscosity liquid in the center. Reference [9] analyzes the stability of CAF numerically, neglecting surface tension. They find the system is stable provided the inner fluid is the more viscous and also as long as the inner-to-outer fluid thickness ratio exceeds a critical value. Reference [14] determined the linear stability of the system when surface tension effects are included. They found for some viscosity ratios, where the inner fluid was more viscous, a band of stable base-flow strengths exists. In this instance, the destabilizing effects of surface tension to long waves are dampened by the interfacial shear resulting from a sufficiently large pressure gradient. However, if the shear is too strong, a surface wave instability renders short waves unstable due to the jump in viscosities at the interface. Reference [15] found that, in the presence of surface tension, the system is always unstable if the outer fluid is the more viscous. For all viscosity ratios considered in Refs. [14,15], axisymmetric modes were found to be the most unstable. However, experimental work carried out in Ref. [16] suggested that nonaxisymmetric disturbances are important if the outer fluid is thin and the inner fluid is the more viscous.

Turning to the RAF configuration, Ref. [2] studied a two-fluid Couette system, in the absence of a pressure gradient, with the fluids contained between coaxial cylinders and with the inner cylinder translating along its axis. They carried out a linear stability analysis, including both axisymmetric and nonaxisymmetric disturbances, and found that axisymmetric modes are the most unstable for the parameters considered. They also showed that the continuous translation of the inner cylinder allows for stability when the outer fluid is the more viscous. In a related study, Ref. [17] examined pressure-driven RAF with the axial rod stationary. Their stability analysis, which also permitted both axisymmetric and nonaxisymmetric disturbances, focused on the case where the inner fluid is the more viscous. They showed that the relative thicknesses of the rod and fluid layers play an important role in determining the stability of the system. Under certain settings the rod in the RAF configuration affords stability for a larger window of viscosity ratios than in ordinary CAF, and interfacial modes that ordinarily derive from the viscosity difference at the interface can be suppressed. Under certain rod and fluid thicknesses, nonaxisymmetric modes were found to become important at large Reynolds numbers. Here, axisymmetric modes also existed, and these were found to be a continuum from the planar unstable shear modes found by Ref. [18]. These were named shear modes and were shown to be a result of the boundaries and background shear, not an interfacial mode. Reference [19] examined the effect on the classical Rayleigh instability of including a rod along the column's axis and a base flow induced by a pressure gradient in a liquid column surrounded by a gas. They too suggested that nonaxisymmetric modes dominate when the pressure gradient is large. They found that when the liquid layer is thin, the base flow can dampen destabilizing capillary effects, and that the optimal width of the annular gap for stabilization depends on the pressure gradient, although complete stabilization is not possible. Reference [1] studied the

stability of a viscous fluid thread that is driven by an axial pressure gradient through a pipe with a translating rod along its axis. They found that nonaxisymmetric perturbations are the most unstable, and that linear stability for all Reynolds numbers is obtained when the rod velocity exceeds a critical value. Subsequently, and for the same configuration, Ref. [20] numerically computed axisymmetric traveling-wave solutions for arbitrary Reynolds number. They found that increasing the rod velocity always has a stabilizing effect on axisymmetric deformations. Reference [21] examined Poiseuille flow through the annular gap between two coaxial cylinders. He found that the cylinder radius ratio is crucial in determining stability and that, under the right conditions, nonaxisymmetric modes can be the most unstable. A single fluid can be viewed as a special case of the two-fluid problem when the viscosities are equal and there is no surface tension. For axisymmetric and nonaxisymmetric disturbances, respectively, Refs. [22,23] investigated the role played by an insoluble surfactant in the two-fluid RAF problem, allowing for a nonzero rod velocity. In the latter paper it was found that, for some parameter sets, the flow can be stable to axisymmetric disturbances but unstable to nonaxisymmetric disturbances.

In the light of these various findings, it appears plausible that including an axial rod may have a stabilizing effect on CAF, when the outer fluid is more viscous, but that nonaxisymmetric modes may be dangerous and should certainly be included in any analysis. In the present work we extend previous investigations of RAF to allow for a more viscous outer fluid as well as the axial translation of the rod. We allow for both axisymmetric and nonaxisymmetric perturbations. Of particular interest is to identify stable configurations with potential implications for practical applications. First, in Sec. IV A we consider a pressure-driven flow and a stationary rod. A more viscous inner fluid is examined in Sec. IV A 1, extending the work of Ref. [17] to other parameter ranges, while a more viscous outer fluid is examined in Sec. IV A 2. In Sec. IV B we allow the rod to translate at constant speed along its axis, either in the same direction as the driving pressure-driven flow or against it. A more viscous inner fluid is considered in Sec. IV B 1 and a less viscous inner fluid in Sec. IV B 2.

While an analytical solution that determines the perturbation growth rates is possible in the Stokes flow limit, in general the stability problem presents a generalized eigenvalue problem that must be solved numerically, and this is done using a spectral method and an in-built eigenvalue problem solver in matlab. Both when it is stationary and when it is in motion, the axial rod is found to make a significant difference to the system's stability, when compared to its CAF counterpart. Novel results are found for RAF, and it is shown that nonaxisymmetric modes can be the most unstable for both a stationary and a moving rod. The results highlight the intricate balance and interplay of forces—namely, shear stress, surface tension, and friction—and their collective role in dictating the stability dynamics of the system.

II. FORMULATION

The flow of two incompressible, immiscible fluids of different viscosities through a circular cylindrical pipe centered around a rod is considered. We use a cylindrical coordinate system (r, θ, z) , where r and θ are the radial and azimuthal components and z points along the rod. The rod has radius \tilde{R}_0 and the outer wall radius \tilde{R}_2 . The two fluids are arranged in concentric annuli, and in equilibrium the interface is at $r = \tilde{R}_1$, so that fluid 1 occupies $\tilde{R}_0 < r < \tilde{R}_1$ and fluid 2 fills $\tilde{R}_1 < r < \tilde{R}_2$. The fluids are assumed to have the same density, $\tilde{\rho}$, so that gravity does not affect the system. The flow is driven by a pressure gradient applied along the pipe of magnitude \tilde{G} , and the rod translates along the z axis with speed \tilde{W} , which can be of either sign or zero. As a result an axial base flow, $\tilde{w}_1(r)$ and $\tilde{w}_2(r)$, is generated in fluids 1 and 2, given in nondimensional form in Eqs. (10) and (11). A schematic of the base state is shown in Fig. 1.

We nondimensionalize the problem using the length scale \tilde{R}_1 , the velocity scale $\tilde{\sigma}/\tilde{\mu}_1$, the pressure scale $\tilde{\sigma}/\tilde{R}_1$, and the timescale $\tilde{R}_1\tilde{\mu}_1/\tilde{\sigma}$, where $\tilde{\sigma}$ is the coefficient of surface tension at the interface and $\tilde{\mu}_\iota$ the fluid viscosities, where $\iota = 1, 2$ for fluids 1 and 2, respectively. The Navier-Stokes equations apply in both fluids, with continuity of velocity and stress at the interface and solid

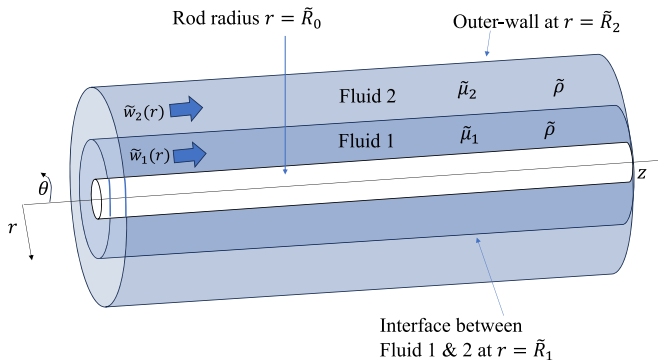


FIG. 1. Schematic of the base state.

boundary conditions at the rod and wall. We denote the nondimensional pressure and velocity by p and $\mathbf{u} = (u, v, w)^T$, where u , v , and w are respectively the radial, azimuthal, and axial components. From here on r and z take dimensionless form. The following six dimensionless parameters appear in the nondimensionalized governing equations: R_0 and R_2 denote the dimensionless rod radius and the outer-wall radius,

$$\mu = \frac{\tilde{\mu}_2}{\tilde{\mu}_1} \quad (1)$$

is the viscosity ratio of the fluids,

$$G = \frac{\tilde{\rho} \tilde{G} \tilde{R}_1^3}{\tilde{\mu}_1^2} \geq 0 \quad (2)$$

measures the strength of the driving pressure gradient,

$$W = \frac{\tilde{\rho} \tilde{W} \tilde{R}_1}{\tilde{\mu}_1} \leq 0 \quad (3)$$

is the magnitude of the axial velocity of the rod (which can take either sign), and

$$J = \frac{\tilde{\rho} \tilde{R}_1 \tilde{\sigma}}{\tilde{\mu}_1^2} \quad (4)$$

is a measure of the strength of capillary forcing. We note that J is the inverse square of the Ohnesorge number $\text{Oh} = \tilde{\mu}_1 / (\tilde{\rho} \tilde{R}_1 \tilde{\sigma})^{1/2}$, and differs by a factor of $(\tilde{R}_1 - \tilde{R}_0) \tilde{R}_2 / \tilde{R}_1^2$ from the J^* defined in Ref. [17]. Each of G , J , and W can be considered as a Reynolds number based on different scales. We choose to nondimensionalize velocity with respect to the capillary scale in order to focus on the interface behavior. In dimensionless variables, the Navier-Stokes equations applied in each fluid are

$$J \frac{D\mathbf{u}_i}{Dt} + \nabla p_i = \mu^{(i)} \nabla^2 \mathbf{u}_i, \quad \nabla \cdot \mathbf{u}_i = 0, \quad (5)$$

where D/Dt denotes the material derivative, and

$$\mu^{(1)} = 1, \quad \mu^{(2)} = \mu. \quad (6)$$

The stress condition at the interface is

$$[\mathbf{T}_i \cdot \mathbf{n}] = (\nabla \cdot \mathbf{n}) \mathbf{n}, \quad (7)$$

where \mathbf{T}_i is the dimensionless stress tensor, given by

$$\mathbf{T}_i = -p_i \mathbf{I} + \mu_i (\nabla \mathbf{u}_i + (\nabla \mathbf{u}_i)^T). \quad (8)$$

The square brackets denote the jump across the interface of the two fluids, and \mathbf{n} is the unit normal vector to the interface. In general, the interface between the two fluids takes the form $r = R(\theta, z, t)$, and the usual kinematic equation,

$$\frac{D}{Dt}(R(\theta, z, t) - r) = 0, \quad (9)$$

is applied at $r = R$. Additionally, continuity of \mathbf{u}_i at the boundaries and interface is required. The nondimensionalized base flow is solely in the axial direction, with functional form $\bar{w} = Ar^2 + B \log r + C$, where the constants take different values in the two fluids. Explicitly, it is given in fluids 1 and 2, respectively, by

$$\bar{w}_1 = \frac{G}{4J} \left(R_0^2 - r^2 + a \ln \frac{r}{R_0} \right) + \frac{W}{J} \left(1 - b \ln \frac{r}{R_0} \right), \quad (10)$$

$$\bar{w}_2 = \frac{G}{4\mu J} \left(R_2^2 - r^2 + a \ln \frac{r}{R_2} \right) - \frac{Wb}{\mu J} \ln \frac{r}{R_2}, \quad (11)$$

where

$$a = \frac{R_2^2 - 1 + \mu(1 - R_0^2)}{\ln R_2 - \mu \ln R_0}, \quad b = \frac{\mu}{\ln R_2 - \mu \ln R_0}. \quad (12)$$

Viewed as a single function $\bar{w}(r)$, the velocity is continuous but has a jump in gradient at $r = 1$ if $\mu \neq 1$. This has implications for the stability behavior at high Reynolds number, as some profiles $\bar{w}(r)$ may be prone to an inflection-like inviscid instability. The nondimensionalized pressure in the base state is given by

$$\bar{p}_1 = -\frac{Gz}{J} + p_c + 1, \quad \bar{p}_2 = -\frac{Gz}{J} + p_c, \quad (13)$$

where p_c is a reference pressure that can be taken to be zero, and the third term in \bar{p}_1 is the result of surface tension. We now determine the linear stability of the base state.

III. LINEAR STABILITY ANALYSIS

In the base state the interface is located at $r = 1$. We consider a small disturbance such that the interface becomes

$$r = 1 + \varepsilon \mathcal{R}(S\zeta), \quad (14)$$

where $\zeta = \exp(ikz + m\theta) + st$, $\varepsilon \ll 1$, k, m are real wave numbers with m an integer, $s \equiv s_r + is_i$ is the complex growth rate, and S is a constant which, if nonzero, can be normalized to unity. We retain S in the problem to allow for eigenfunctions with $S = 0$. The real part of the perturbation is taken in Eq. (14), and this is assumed from here on for the perturbations of all variables, but is not written explicitly. An appropriate expansion for the velocity and pressure is assumed to be

$$p_i = \bar{p}_i(z) + \varepsilon \zeta \hat{p}_i(r), \quad u_i = \varepsilon \zeta \hat{u}_i(r), \quad v_i = \varepsilon \zeta \hat{v}_i(r), \quad w_i = \bar{w}_i(r) + \varepsilon \zeta \hat{w}_i(r), \quad (15)$$

where we drop the hats of the perturbation variables hereafter. Substituting Eqs. (15) into the dimensionless Navier-Stokes equations and linearizing, we obtain

$$(ru_i)' + imv_i + ikrw_i = 0, \quad (16)$$

$$J(s + ik\bar{w}_i)r^2u_i + r^2p_i' = \mu^{(i)}(-2imv_i - u_i + r^2u_i'' + ru_i' - (m^2 + k^2r^2)u_i), \quad (17)$$

$$J(s + ik\bar{w}_i)r^2v_i + imrp_i = \mu^{(i)}(-v_i + 2imu_i + r^2v_i'' + rv_i' - (m^2 + k^2r^2)v_i), \quad (18)$$

$$J(u_i\bar{w}_i' + (s + ik\bar{w}_i)w_i)r^2 + ikr^2p_i = \mu^{(i)}(r^2w_i'' + rw_i' - (m^2 + k^2r^2)w_i), \quad (19)$$

where $'$ denotes to the derivative with respect to r .

For Stokes flow, $J \rightarrow 0$ while keeping $G = O(J)$, $\bar{w}_l = O(1)$. In this limit, Eqs. (16)–(19) have an analytical solution. The base flow then only contributes to the imaginary part of the growth rate as expected from the reversibility of the Stokes problem [8], and confirmed analytically. Consequently, to allow for base-flow effects, the full system must be considered, which in general requires numerical solution.

After the disturbance, the normal stress condition at the interface gives

$$p_1 - p_2 + 2(\mu u'_2 - u'_1) + (1 - m^2 - k^2)S = 0, \quad (20)$$

and continuity of the axial and azimuthal tangential stress gives

$$iku_1 + w'_1 = \mu(iku_2 + w'_2), \quad (21)$$

$$imu_1 - v_1 + v'_1 = \mu(imu_2 - v_2 + v'_2). \quad (22)$$

Continuity of \mathbf{u} at the interface results in

$$u_1 = u_2, \quad v_1 = v_2, \quad w_1 + \bar{w}'_1 S = w_2 + \bar{w}'_2 S. \quad (23)$$

The kinematic condition at the interface requires

$$sS - u_t + ik\bar{w}_l S = 0. \quad (24)$$

Equations (20)–(24) are all applied at $r = 1$. Finally, no slip at the outer wall and rod gives

$$u_2(R_2) = 0, \quad v_2(R_2) = 0, \quad w_2(R_2) = 0, \quad (25)$$

and

$$u_1(R_0) = 0, \quad v_1(R_0) = 0, \quad w_1(R_0) = 0, \quad (26)$$

respectively. Importantly, the stability problem for RAF does not recover that for CAF upon taking the limit $R_0 \rightarrow 0$ [14,17] as the appropriate boundary conditions on the axis are not the same. More generally, even if we set the rod velocity to be equal to that of the CAF base flow at the rod radius, the two stability problems are different because of the differing boundary conditions for the perturbations. The results for a single fluid can be found by setting $\mu = 1$ and letting $J \rightarrow 0$ while rescaling s and the perturbed variables with $1/J$.

A. Numerical methods

The system of equations (16)–(26) forms an eigenvalue problem for s , where $s_r > 0$ corresponds to an unstable mode, and if for all modes $s_r \leq 0$ then the system is (neutrally) stable. Following Ref. [14] we use a pseudospectral method to solve the system of equations numerically. We eliminate $p(r)$, using the axial momentum equation to give one continuity equation and two momentum equations applied in each fluid, along with 13 boundary conditions (20)–(26). We introduce a truncated series of Chebyshev polynomials $T_n(x)$ for the flow variables, such that

$$(u_t, v_t, w_t) = \sum_{n=0}^{N_t} (a_n, b_n, c_n) T_n(x), \quad (27)$$

where each fluid region is mapped onto the canonical interval $-1 \leq x \leq 1$ using

$$x = \frac{(r-1) + (r-R_0)}{1-R_0}, \quad x = \frac{(r-1) + (r-R_2)}{R_2-1}, \quad (28)$$

in fluids 1 and 2, respectively. We substitute the expansions (27) into the momentum and continuity equations, Eqs. (16)–(19) enforcing these at interior shifted Gauss-Lobatto collocation points given as $x_l = \cos(\pi(l-1/2)/N)$, for $l = 1, \dots, N$, with $N = N_1 - 1$ and $N = N_2 - 1$ in fluids 1 and 2, respectively. Similarly, we substitute Eq. (27) into Eqs. (20)–(26) and enforce these at $x = \pm 1$ as

required for each fluid. This results in $3(N_1 + N_2 + 2)$ unknown Chebyshev coefficients stored in the vector \mathbf{v} , along with the surface deformation S , such that

$$\mathbf{A}\mathbf{v} = s\mathbf{B}\mathbf{v}, \quad (29)$$

where \mathbf{A} and \mathbf{B} are $(3(N_1 + N_2) + 7) \times (3(N_1 + N_2) + 7)$ matrices with known elements. The first $3(N_1 + N_2 - 2)$ rows account for the radial and azimuthal momentum equation and the continuity equation applied at $N_1 - 1$ and $N_2 - 1$ collocation points in fluids 1 and 2, respectively, and the last 13 rows account for Eqs. (20)–(26). We solve Eq. (29) using the matlab routine *eigs* to find the eigenvectors and corresponding values of s . To ensure reliability, we restrict attention to no more than half of the modes produced, ordered by eigenvalue size.

In the absence of a rod, Ref. [14] reported the occurrence of spurious eigenvalues. We can replicate this finding using the appropriate base flow for no rod, and replacing Eq. (26) with the centerline conditions given by Ref. [14]. We also find nonconvergent spurious eigenvalues in the rod annular problem. These are removed from consideration by carefully identifying those eigenvalues which converge as $N_{1,2}$ increases. Taking $90 \leq N_{1,2} \leq 140$ we find accurate results except for very large values of J , G , and R_2 , when an increase in N_i is needed. The numerical results are compared with the growth rate for the analytical solution in the Stokes regime, with the values provided by Ref. [23] for no surfactant and a moving rod, and with a small- k analysis (see Sec. III C), all with excellent agreement. We also reproduce the $m = 0, 1$ neutral curves in Figs. 5–7 of Ref. [17], and the neutral curves in Fig. 5(a) of Ref. [2].

B. Inviscid limit

Before presenting the results, we make some observations on the base-flow structure and its likely implications. Our scaling is not convenient for the inviscid limit, for which W , G , and $J^{1/2} \rightarrow \infty$ at the same rate while s and the perturbed velocity scale as $J^{-1/2}$, but p is $O(1)$. Physically, in the limit of both fluids becoming inviscid, and in the absence of surface tension, one might expect the stability behavior to be the same as that for a single fluid with velocity profile $\bar{w}(r)$, which has a discontinuous derivative at $r = 1$. Neglecting for now this discontinuity, there is an analog of Rayleigh's inflection point criterion for two-dimensional (2D) flow, namely, that a necessary condition for axisymmetric inviscid instability is that it should change sign somewhere in $R_0 < r < R_2$ [24]. If the flow is inviscidly unstable, then there will be a window of unstable k of nonzero width. If, however, the flow is inviscidly stable, then we would expect any instability of the slightly viscous problem only to appear as $k \rightarrow 0$. The addition of surface tension is unlikely to affect these long waves, though it may limit the unstable k range for an inviscid instability.

Considering now the kink at $r = 1$, analogy with 2D flow suggests the inviscid flow stability will be the same as that for an infinitesimally modified smooth profile, $\hat{w}(r)$. If such a profile has single-signed $(\hat{w}'/r)'$ we would expect the discontinuous profile also to be inviscidly stable. For our two-fluid profile, $(\bar{w}'/r)'$ is determined solely by the logarithmic term in Eq. (10) and has the same sign in both fluids due to the continuity of $\mu_i \bar{w}'_i$. Whether or not the smoothed profile $(\hat{w}'/r)'$ will have the same sign at $r = 1$ as $(\bar{w}'/r)'$ depends on whether \bar{w}'/r increases across $r = 1$, which is the same as whether \bar{w}' increases. This depends on whether or not $\mu > 1$, with allowance made for the sign of $\bar{w}'(1)$. Now in Eq. (10) the sign of $(\bar{w}'/r)'$ is given by

$$\xi_1 \equiv G(R_2^2 - R_0^2\mu + \mu - 1) - 4\mu W. \quad (30)$$

Whether \bar{w}'/r increases across $r = 1$ is determined by the sign of

$$\xi_2 \equiv (\mu - 1)[G(R_2^2 - R_0^2\mu + \mu - 1 - 2 \ln R_2 + 2\mu \ln R_0) - 4\mu W]. \quad (31)$$

Inviscid stability requires ξ_1 and ξ_2 to have the same sign. If this condition is violated, instability usually occurs, although it should be remembered that it is not strictly guaranteed [25]. It should also be noted that for a sufficiently large rod velocity of either sign the inviscid stability is determined by $\mu \leq 1$. When $\mu = 0$, we always have instability.

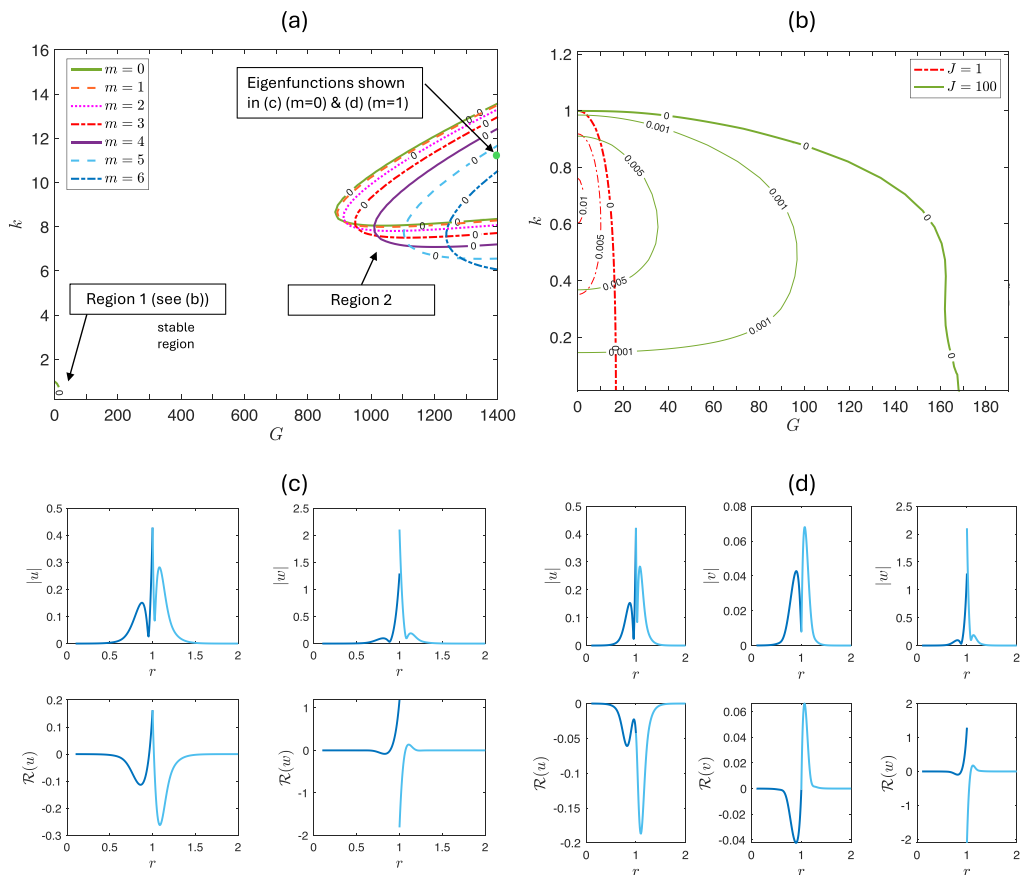


FIG. 2. Growth rate contours $s_r(G, k)$ when $\mu = 0.5$, $R_0 = 0.1$, $R_2 = 2$, and $W = 0$. (a) $m = 0, 1$ for $J = 1$. (b) $m = 0$ for $J = 1, 100$. Eigenfunctions for region 2 in panel (a) when $G = 1400$, $k = 11.0$, and in (c) $m = 0$, $s = 0.4626 - 12981.9i$ and (d) $m = 1$, $s = 0.4556 - 12982i$. Region 1 is driven by surface tension, region 2 by interfacial shear. The flow is inviscidly stable, so that region 2 disappears as J increases.

It is also possible to develop similar criteria for modes with $m > 0$, but these are a little more complicated and it seems simpler to solve the entire system for large G numerically.

C. Long-wave limit

The equations simplify in the limit $k \rightarrow 0$, keeping the other parameters $O(1)$. We can expand

$$(u_t, v_t, kw_t) = k\mathbf{u}_{t1} + k^2\mathbf{u}_{t2} + \dots, \quad p_t = k^{-1}p_{t0} + p_{t1} + \dots, \quad s = ks_1 + k^2s_2 + \dots \quad (32)$$

The analysis is the same as in Ref. [17] apart from the inclusion of the rod velocity, W . For $m = 0$ we find s_1 is imaginary and at leading order

$$s_r = k^2 \left[\alpha - \frac{1}{J}(\beta G^2 + \gamma W^2 + \delta WG) \right], \quad (33)$$

where $\alpha, \beta, \gamma, \delta$ are known in terms of R_0, R_2 , and μ . The constants α and β are given in Eq. (15) of Ref. [17]. When $W = 0$, Eq. (33) agrees with the boundary of the instability region around $G = k = 0$, for example, in Fig. 2(b) below. If $\beta/\alpha \leq 0$ axisymmetric short waves are always unstable. When $W \neq 0$, there can be two positive roots for G , in which case the instability window

shifts to larger G as indeed we will find in Fig. 10(b). As J varies, Eq. (33) predicts the observed square root dependency on J of the critical G values.

IV. RESULTS

The problem is defined by the parameters R_0, R_2, μ, J, G, W and wavenumbers (k, m). For fixed k and m we find at most one unstable mode.

A. Stationary rod: $W = 0$

Here we outline the results for a stationary rod, $W = 0$. The system is identical to that studied in Ref. [17] and we find agreement with the conclusions presented. When the inner fluid is more viscous, Ref. [17] finds that for certain parameters and large base-flow strengths, $m = 1$ modes are rendered unstable before $m = 0$ modes, as the Reynolds number is increased. In Sec. IV A 1 we investigate these modes further for other parameter values. In Sec. IV A 2 we consider the outer fluid as more viscous. In this case, the system is always unstable for ordinary CAF [15], yet we find for RAF, if the rod thickness exceeds a critical value, regions of stability can be found.

1. $\mu < 1$: More viscous inner fluid

As expected from Ref. [17], there exists a window of base-flow strengths, G , where the system is stable for a range of parameter values. We define G_L and G_R as critical values of G , such that there is a band of stability given by $G_L < G < G_R$. Reference [17] finds that at low base-flow strengths, axisymmetric modes are the most unstable, and Fig. 2 gives an example configuration where $m = 0$ modes are the most unstable. Two regions of instability exist when $J = 1$; regions 1 and 2. Region 1 is unstable only to axisymmetric modes with $k \leq 1$, as these are essentially capillary modes which the flow is too weak to control. Increasing J increases the growth rate of the instability, and region 1 grows larger as $G_L \propto \sqrt{J}$ as given by Eq. (33) [see Fig. 2(b)]. Region 2 is unstable for moderately large k and various m . The eigenfunctions shown in Figs. 2(c) and 2(d) display a localized behavior to the interface of the two fluids, representing the short-wave instability discussed by Refs. [14] and [17]. This is caused by the viscosity jump, and they are named “interface modes” in Refs. [17, 18]. Indeed, increasing the viscosity ratio pushes region 2 to the right, so that at $\mu = 0.9$ there is stability up to at least $G = 2 \times 10^4$, when $J = 1$. Moreover, as J increases so does G_R , and region 2 is moved to the right and may disappear entirely. When $J = 100$ in Fig. 2 we have complete stability up to at least $G = 6.5 \times 10^4$, which is consistent with the base flow being inviscidly stable.

As R_2 is decreased, the situation is more involved with nonaxisymmetric modes dominating for $G \geq G_c$ and $J \geq J_c$. In Fig. 3 $R_2 = 1.3$ compared to $R_2 = 2$ in Fig. 2, while μ and R_0 remain the same. Figure 3(a) shows that when $J = 1$ regions 1 and 2 exist, and increasing J causes region 2 to move to the right, as when $R_2 = 2$. Indeed, when $J = 100$ in Fig. 3(b) region 2 is stabilized, but a third region of instability exists for $G \geq G_c$, where only $m = 1$ modes are unstable. We find that G_c is unchanged by increasing J , although the growth rate decreases as $1/J$. The region persists when J is decreased to $J = 1$, but then region 2 modes dominate at flow strengths $G \geq G_c$. This resembles the scenario of Figs. 6 and 7 of Ref. [17], although some care in interpretation is needed because of the different nondimensionalization used. As R_0 increases, keeping Ref. [17] other variables constant, it appears that region 2 moves to the right. However, in terms of our scaling, this entails a simultaneous increase of surface tension, J , which is the physical reason for the stabilization of region 2 for fixed G .

The eigenfunction shown in Fig. 3(d) corresponds to a point in region 3, and it shows that gradients of the flow in fluid 1 are localized near the rod boundary, while activity occurs throughout the thinner, less viscous fluid 2 layer. In comparing Figs. 2 and 3, we find that the region occurs once we decrease the thickness of the outer, less viscous, fluid. A similar situation occurred for the 2D shear modes in Ref. [18], which were only destabilizing for a thin, less viscous fluid near the wall boundary. This implies that the nonaxisymmetric region 3 modes could also consist of

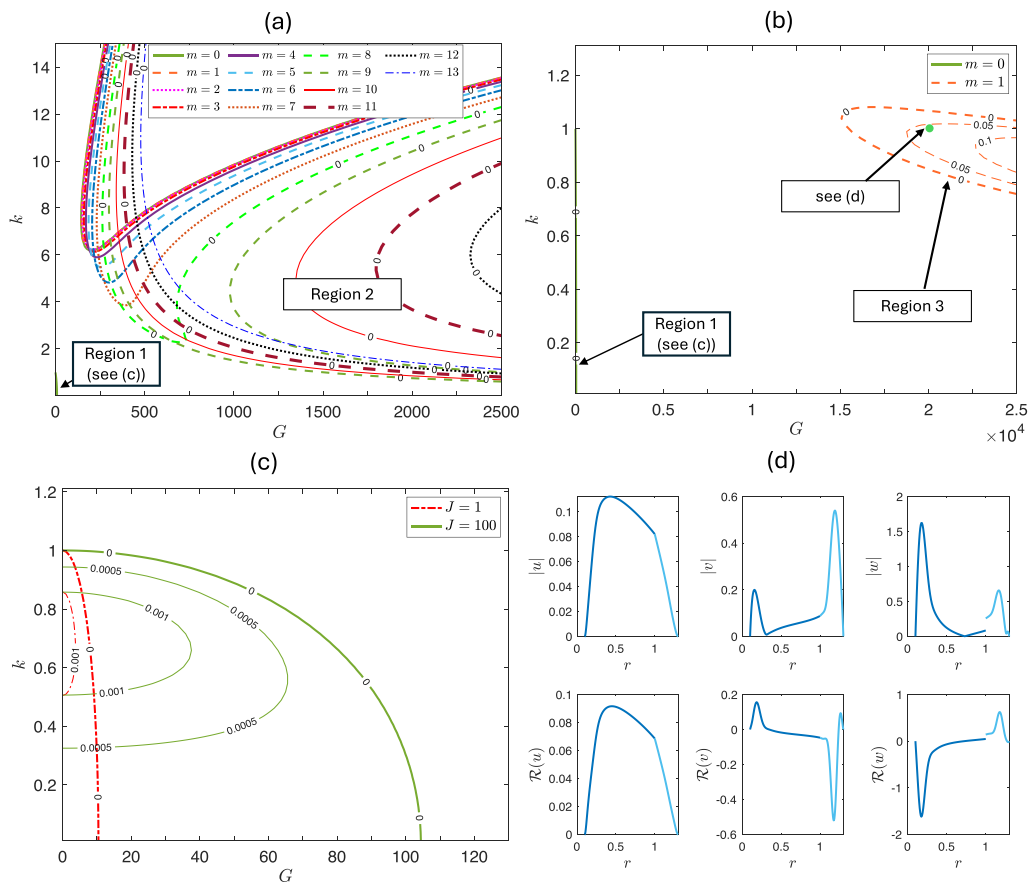


FIG. 3. Growth rate contours $s_r(G, k)$ for $\mu = 0.5$, $R_0 = 0.1$, $R_2 = 1.3$, and $W = 0$. (a) $J = 1$; regions 1 and 2 exist. (b) $J = 100$; regions 1 and 3 exist (region 2 has been stabilized). (c) Region 1, with $m = 0$ modes unstable, for $J = 1, 100$. (d) The eigenfunction at $(G, k) = (2 \times 10^4, 1)$ for $m = 1$ (this has the growth rate $s = 0.059 - 19.29i$ whose real part is near maximum). The eigenfunction is most active away from interface, so that J has limited influence.

shear modes. To support this statement, we refer to Ref. [17], who considered the stability of single-fluid Poiseuille flow in an annular pipe. In Ref. [17] Fig. 1 it is shown that, for a single fluid, as the strength of the flow increases, one of the set of $m = 0, 1, 2, 3$ modes is made unstable first, depending on the ratio of the inner and outer pipe radii. We observe similar behavior in our two-fluid problem, and find that varying R_0 and R_2 can produce similar results, with other m modes rendered unstable at sufficiently high G , and with similar eigenfunctions. The effect of narrowing the annular gap is demonstrated in Fig. 4. In Fig. 4(a), $R_0 = 0.45$ and $R_2 = 1.1$ (cf. Fig. 3, where $R_0 = 0.1$ and $R_2 = 1.3$). Here, $m = 0$ is unstable in region 1, but there also exists a region where $m = 2$ is the only unstable mode, and the corresponding eigenfunctions [see Fig. 4(b)] resemble those of region 3 in Fig. 3. In Fig. 4(c), the rod radius is set at $R_0 = 0.1$, and here we see a case where $m = 0$ modes become unstable first with modes $m > 0$ losing stability at successively higher G . The eigenfunction for the $m = 0$ mode is shown in Fig. 4(d). Its axial component is typical for region 3, but the radial velocity exhibits a localized behavior towards the inner boundary in fluid 1, whereas in fluid 2 there is a sharp drop from the interface to the outer wall. The eigenfunction for the $m = 1$ mode has azimuthal and axial components resembling those in Fig. 3(d), but the radial

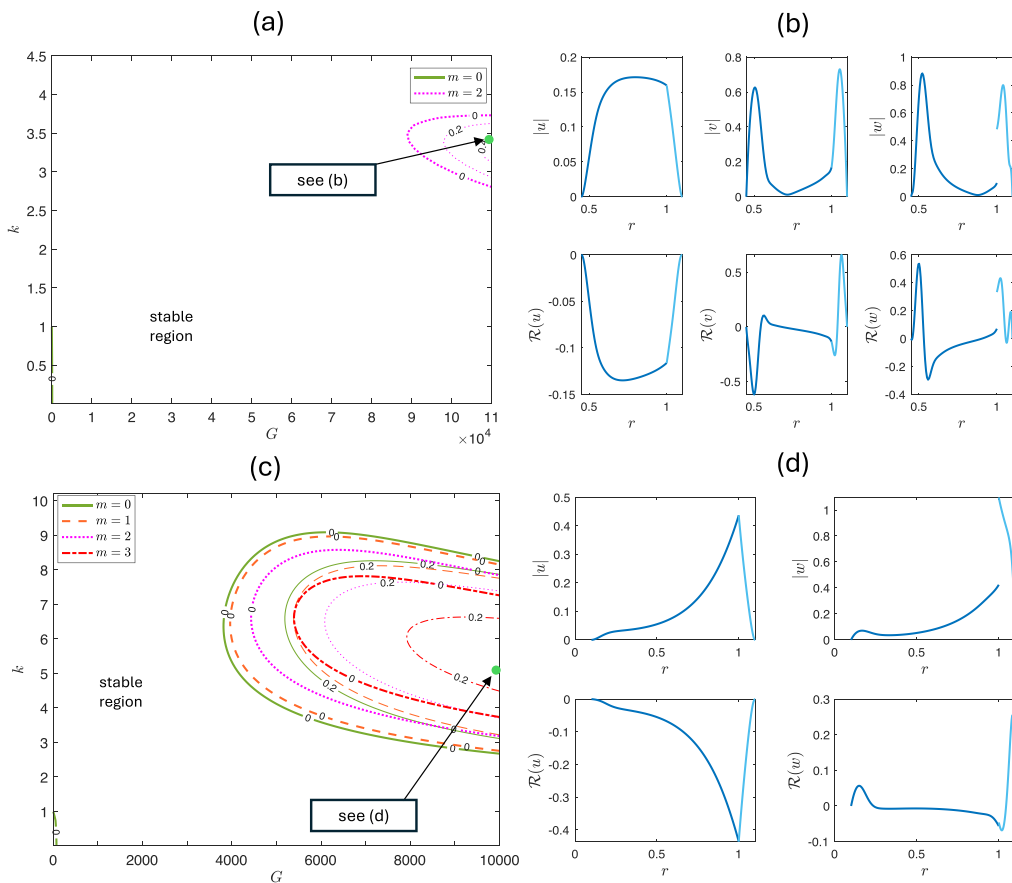


FIG. 4. Growth rates, $s_r(G, k)$, and eigenfunctions, for $\mu = 0.5$ and $J = 100$. (a) Growth rates plotted when $R_0 = 0.45$, $R_2 = 1.1$, and $W = 0$, and (b) the eigenfunction at $(G, k) = (110000, 3.5)$ for $m = 2$ ($s = 0.37 - 90.81i$). (c) Growth rates plotted when $R_0 = 0.1$ and $R_2 = 1.1$ and (d) the eigenfunction at $(G, k) = (10^4, 5.5)$ for $m = 0$ ($s = 0.785 - 32.619i$).

part is different. Moreover, for low G in this region, increasing J can stabilize modes. Yet at higher G , say $G = 2 \times 10^4$, unstable modes still exist, and seem to be mostly unaffected by increasing J , in a similar manner to region 3 in Figs. 3(d) and 4(b).

We find that the existence of region 3 is very sensitive to the choice of $\mu < 1$, R_0 , and R_2 . Increasing these three parameters independently, we find that region 3 shifts to the right from its position in Fig. 3(b), thereby increasing G_c . On the other hand, varying J does not change the location of region 3 much, suggesting that surface tension is not important for this instability, which is unlikely to be due to interfacial modes. This, coupled with the work of Refs. [17, 18, 21], would suggest that even the nonaxisymmetric region 3 instabilities are a result of the pipe geometry and background shear, rather than interfacial friction or capillarity, and occur for specific fluid thicknesses.

Furthermore, decreasing the outer-wall radius, from $R_2 = 2$ in Fig. 2 to $R_2 = 1.3$ in Fig. 3, decreases G_L , for both $J = 1$ and $J = 100$. Yet G_R also decreases when $J = 1$, resulting in a smaller range of stable G as R_2 decreases. If R_0 is increased to 0.45 the three regions of instability still exist, but occur for different ranges of G . Increasing the rod radius increases G_L , G_R , and G_c . Thus, for small G a smaller rod radius would be favorable, yet the converse is true at higher G . Here, and

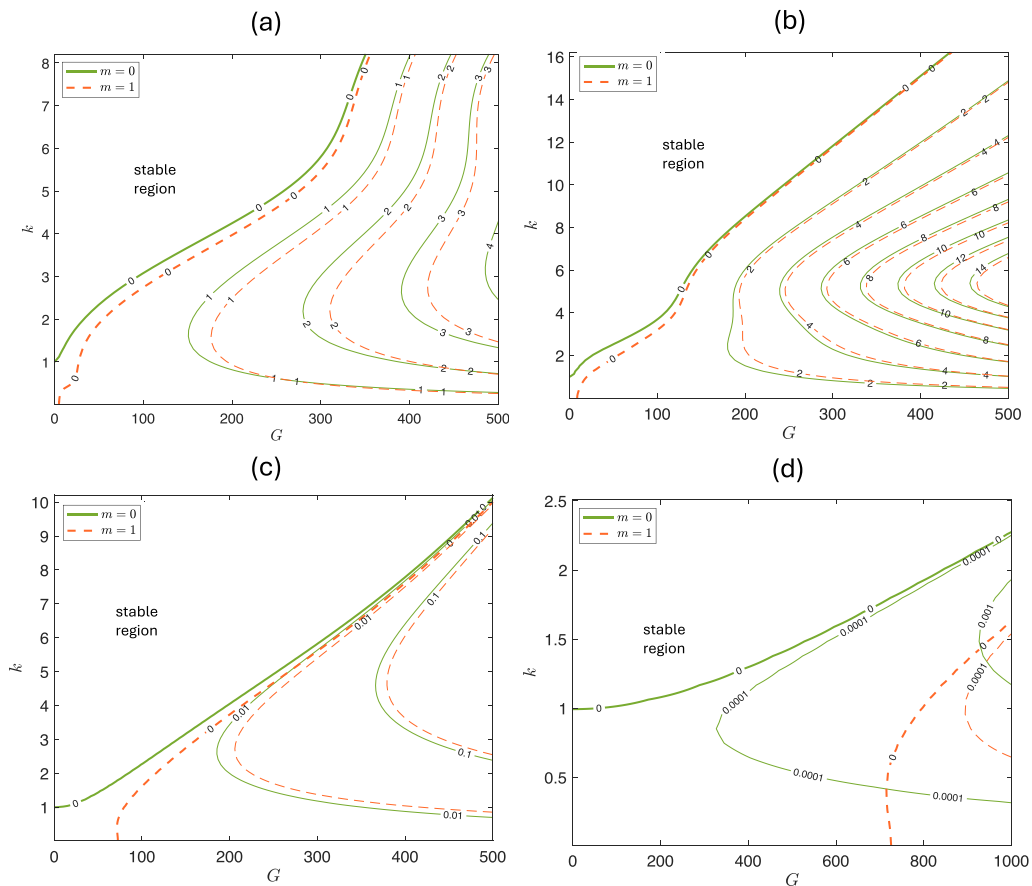


FIG. 5. Growth rates $s_r(G, k)$ showing instability for all G when $\mu = 0.5$ and $W = 0$. (a) $J = 1$, $R_0 = 0.1$, and $R_2 = 2.5$. (b) $J = 1$, $R_0 = 0.45$, and $R_2 = 2$. (c) $J = 1$, $R_0 = 0.9$, and $R_2 = 1.3$. (d) $J = 100$, $R_0 = 0.9$, and $R_2 = 1.3$. When J increases, short waves are stabilized, but the system remains unstable. Both $m = 0$ and $m = 1$ are unstable, but $m = 0$ has the largest growth rate. In all of the panels the base-flow profile is inviscidly unstable and $\beta/\alpha < 0$ so all axisymmetric short waves are unstable according to Eq. (33).

in general, G_L is increased as J is increased, and region 2 is shifted to the right as J is increased. Therefore, when G is small, a smaller value of J is favorable to achieve a stable system. However, if there exists a stable band of G , J can be increased to dampen unstable modes provided that the base flow is sufficiently strong and $G < G_c$. For certain conditions, dependent on R_2 and R_0 , a large base-flow strength risks nonaxisymmetric modes becoming unstable, despite an increase in J . Nevertheless, given a prescribed $G > G_c$, increasing R_2 or R_0 can stabilize nonaxisymmetric modes. For example, when R_2 is increased from $R_2 = 1.3$ in Fig. 3 to $R_2 = 2$ in Fig. 2, region 3 does not exist up to at least $G = 6.5 \times 10^4$.

When either the outer-wall radius or the rod radius exceeds a critical value, we found that there are no windows of stability in G . In fact the system is unstable for all of the values of G and J that we examined. Four examples are shown in Fig. 5. In Fig. 5(a) we see that the stability windows in Figs. 2 and 3 have been closed by increasing the outer-wall radius to $R_2 = 2.5$ (with the other parameters fixed). In Fig. 5(b), increasing the rod thickness to $R_0 = 0.45$ has rendered all modes unstable, when the system was stable for $R_0 = 0.1$ in Fig. 2. Similarly, increasing the rod radius to $R_0 = 0.9$ in Fig. 5(c) renders all modes unstable, when for these parameters the system was stable

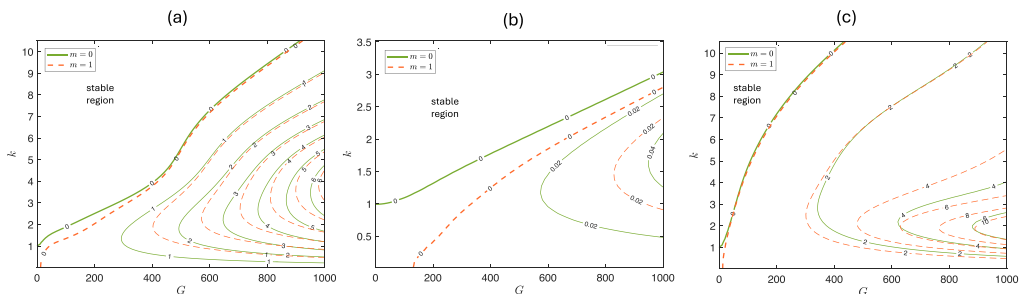


FIG. 6. Growth rates $s_r(G, k)$ for $\mu = 1.5$, $R_0 = 0.1$, and $W = 0$. (a) $R_2 = 2$ and $J = 1$. (b) $R_2 = 2$ and $J = 100$. (c) $R_2 = 1.3$ and $J = 1$. For these parameter values, the system is always unstable, but increasing J stabilizes short waves. Modes with $m > 1$ are also unstable with a smaller growth rate and at larger G_c . For all of the panels the base-flow profiles are inviscidly unstable and $\beta/\alpha < 0$ in Eq. (33).

for $R_0 = 0.45$. In fact, we did not find a stable configuration when $R_0 = 0.9$ and $\mu < 1$, suggesting the system is unstable when the ratio between the rod radius and the inner fluid thickness exceeds a critical value. Lastly, although increasing J widens the band of stable G values for systems that already exhibit regions of stability, when the system is unstable for all G , increasing J will dampen short waves but cannot produce a stable system, as seen when comparing Figs. 5(c) and 5(d). As G increases beyond the displayed range, the neutral curve seems to approach a constant value of k which is determined by the specific parameter values. This agrees with the analysis of Sec. III B, since the base-flow profiles for the parameter sets in Figs. 5(a)–5(d) are unstable in this inviscid limit.

The results shown thus far are for $\mu = 0.5$, and the general trends apply for other values with $\mu < 1$, but for different ranges of parameter values. As Ref. [17] noted, the μ threshold for a stable configuration does indeed increase with the addition of the rod.

2. $\mu > 1$: More viscous outer fluid

For a stationary rod when the outer fluid is more viscous, there exists a critical rod thickness, R_c , where for $R_0 > R_c$ the system can be stabilized for a range of parameter values. It is shown in Fig. 6 that the system is unstable to all base-flow strengths when $R_0 = 0.1$. However, increasing the rod thickness to $R_0 = 0.45$ produces stable regions, as can be seen in Fig. 7, which has otherwise the same parameter values as Fig. 6(a). Figure 7(a) reveals a stability window $G_L < G < G_R$ that separates a band of unstable axisymmetric modes for $0 < G < G_L$, labeled region 1, and a region of unstable modes for $G > G_R$, labeled region 2. Interestingly, for region 2, it is nonaxisymmetric modes which are destabilized first as G increases beyond G_R . The eigenfunctions for $m = 0, 1$ in regions 1 and 2 behave similarly to those in Sec. IV A 1. Figure 7(d) gives an example of an $m = 3$ eigenfunction in region 2, whose behavior is still localized to the interface. Increasing J shifts region 2 to the right, thereby increasing G_R , but simultaneously increasing G_L . Figure 7(b) shows that increasing J from $J = 1$ to $J = 100$ renders larger G unstable in region 1 and increases the growth rate for each G . When $J = 100$, region 2 has been stabilized to at least $G = 10^5$, but another region of instability appears for sufficiently large G , $G > G_c$, shown in Fig. 7(c). Here, $m = 1$ modes are the only unstable modes, and the region exhibits eigenfunctions typical of the instabilities of region 3 in Sec. IV A 1. Note that the greatest activity is in fluid 1, the thinner, less viscous fluid, with a small gradient in fluid 2 near the outer wall. This concurs with the findings of Sec. IV A 1 and Ref. [18]. Thus, increasing J has widened the band of stable G , and when $J = 100$ there is stability between regions 1 and 3. Similarly to Sec. IV A 1, for sufficiently low values of G , a smaller J is preferable for a stable system, whereas high values of G require a larger J . Nevertheless, for $G > G_c$ region 3 remains as J increases, and the growth rate decreases $\propto 1/J$.

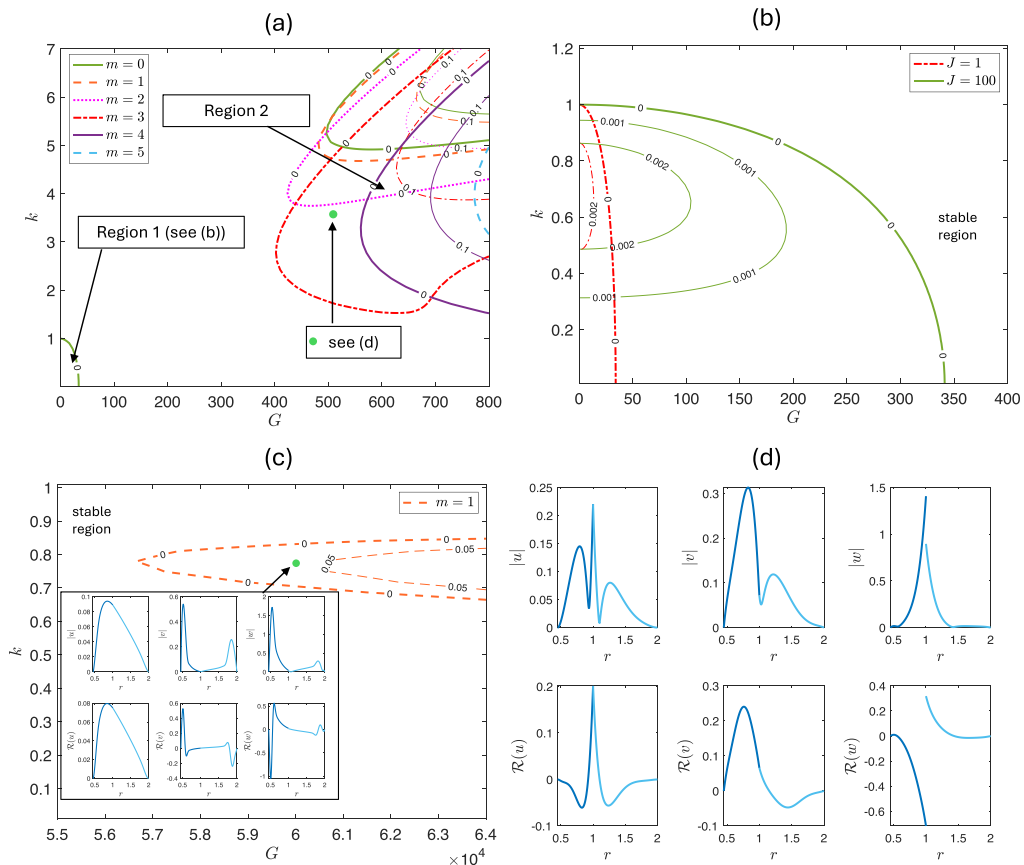


FIG. 7. Growth rates $s_r(G, k)$ for $\mu = 1.5$, $R_0 = 0.45$, $R_2 = 2$, and $W = 0$. (a) $J = 1$ and a band of stable G exists between regions 1 and 2. (b) Enlarged image of region 1 with $m = 0$ isolines for $J = 1$ and $J = 100$. When $J = 100$ there is a band of stable G between region 1 and another region, which is similar to region 3 in Sec. IV A 1. (c) Enlarged view of region 3 for $m = 1$ and $J = 100$; the inset shows the eigenfunction when $s = 0.04-30.1i$, $k = 0.75$, $G = 60000$. (d) The eigenfunction when $J = 1$, $G = 500$, $k = 3.5$, $m = 3$, $s = 0.04163-425.5i$. The eigenfunctions for unstable $m = 0, 1$ modes in regions 1, 2, 3 all behave similarly to those described in Sec. IV A 1.

Increasing R_0 further, from $R_0 = 0.45$ in Fig. 7 to $R_0 = 0.9$ in Fig. 8, renders all modes unstable. Increasing J pushes region 2 in Fig. 8(a) to the right. Once $J = 100$ in Fig. 8(d), we see an increase in J from 1 to 100, which stabilizes $m = 2$ modes, shifts the unstable region for $m = 1$ to the right, and results in a decreased growth rate of the unstable modes. Meanwhile, the unstable region for $m = 0$ expands to larger values of G and exhibits an increased growth rate. When, however, the radius of the outer wall is decreased to $R_2 = 1.3$, stability can be achieved when $R_0 = 0.9$ but not when $R_0 = 0.45$, suggesting that a decrease in R_2 must be matched by an increase in R_0 . A larger stable band of G exists between regions 1 and 2 than in Fig. 7, and we do not see region 3. When $J = 100$, we have stability from $G \approx 1200$ to at least $G = 7 \times 10^4$. This suggests there may be a critical $G_c(R_0, R_2)$ for region 3 to exist when $\mu > 1$ also. Indeed, when retaining the parameters in Fig. 7(c) whereas increasing or decreasing R_0 significantly, G_c increases, but G_c decreases while increasing R_2 and retaining $R_0 = 0.45$. Additionally, increasing μ appears to increase G_c . Although at large G the parameters $R_0 = 0.9$ and $R_2 = 1.3$ favor stability more than the values $R_0 = 0.45$ and $R_2 = 2$ of Fig. 7, the converse is true at low G , due to an increase in G_L . Thus, the optimal geometry

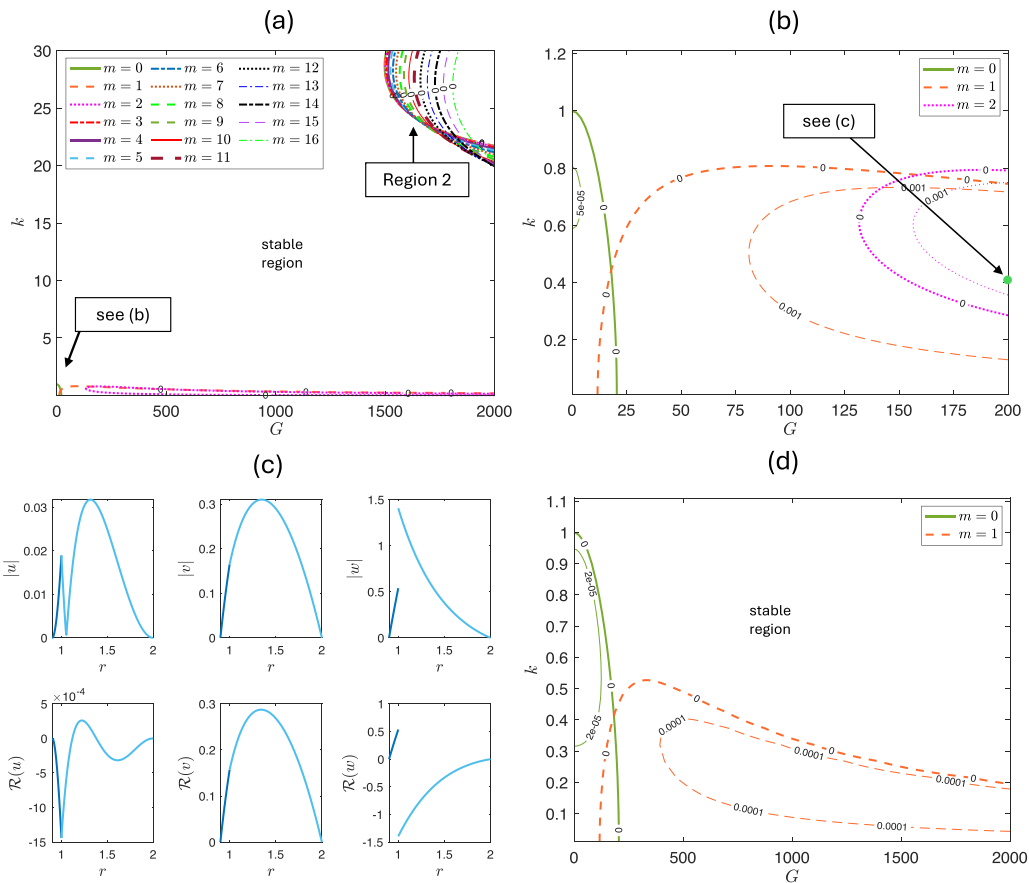


FIG. 8. Growth rates $s_r(G, k)$ and eigenfunction for $\mu = 1.5$, $R_0 = 0.9$, and $R_2 = 2$. (a) $J = 1$, (b) an enlarged image of (a), and (c) an eigenfunction when $G = 200$, $J = 1$, $k = 0.4$, $m = 1$, and $s = 0.005 - 4.029i$. (d) $J = 100$. Increasing J has stabilized region 2 and $m = 2$ modes. As G increases, $k \rightarrow 0$ for unstable m, k modes, since the profile is inviscidly stable.

for stability is determined by the required base-flow strength. Furthermore, as in Sec. IV A 1, once R_2 is sufficiently large, all G will be unstable.

The results shown here for $\mu = 1.5$ hold also for other $\mu > 1$ with different critical values. Interestingly, taking $\mu = 10$, for example, we find that the system is now stable for $R_0 = 0.9$, $R_2 = 2$, whereas it was unstable for $\mu = 1.5$. Regions 1 and 2 exist at low J , and increasing J from $J = 1$ to $J = 100$ widens the range of stable G , but increases region 1, following the trends previously outlined.

B. Moving rod: $W \neq 0$

Translating the rod along its axis with dimensionless velocity W adds another parameter to an already complex system. A moving rod can be stabilizing or destabilizing depending on the parameter values. In Sec. IV B 1 we discuss the effect of the moving rod when the inner fluid is the more viscous, $\mu < 1$, first considering regions 1, 2, and 3, and then configurations that were unstable for all G when $W = 0$. Section IV B 2 contains a corresponding discussion when the outer fluid is the more viscous, $\mu > 1$. In general, moving the rod in the direction of the pressure-driven flow ($W > 0$) is most effective at stabilizing configurations with $\mu < 1$, whereas $W < 0$ is favorable for $\mu > 1$. However, counterexamples can be found as will be described below.

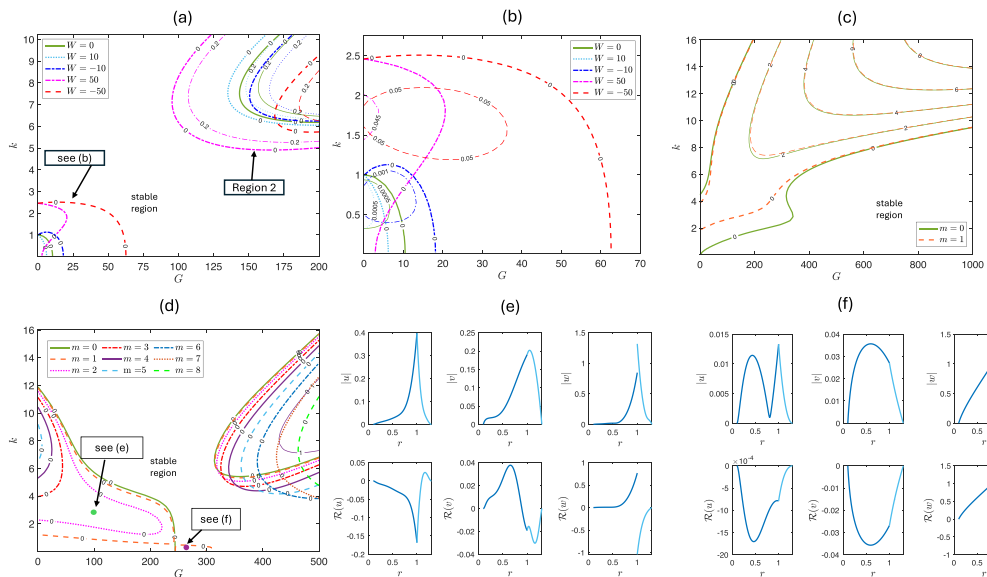


FIG. 9. Growth rates $s_r(G, k)$ for moving rod, $\mu = 0.5$, $R_0 = 0.1$, $R_2 = 1.3$, $J = 1$. (a) Differently shaped $m = 0$ instability regions are found as W varies, as indicated by the $k \rightarrow 0$ result of Eq. (33) for region 1. Region 2 exists for $m \geq 0$ but $m = 0$ has the greatest growth rate. (b) An enlarged image of region 1 in (a). (c) $W = 100$, (d) $W = -200$. Eigenfunctions for points in (d) are given in (e) $W = -200$, $G = 100$, $m = 1$, $k = 3.5$, $s = 1.0522 + 40.006i$ and (f) $W = -200$, $G = 270$, $k = 0.1$, $m = 1$, $s = 0.001105 - 2.578i$. Varying W shifts the regions of instability.

1. $\mu < 1$: More viscous inner fluid

We first discuss the effect of taking $W \neq 0$ on the unstable regions 1, 2, and 3 that were highlighted in Sec. IV A 1. Fixing the parameters as in Fig. 3, we see in Fig. 9 that when $\mu = 0.5$ the unstable regions 1 and 2 both exist for a range of rod speeds W . Figures 9(a) and 9(b) reveal that for small $|W|$, $W > 0$ stabilizes region 1, and $W < 0$ expands it to the right. In contrast, region 2 extends to the left when $W > 0$, and $W < 0$ has a stabilizing effect, pushing region 2 to the right. When $|W|$ is taken to be sufficiently large, there is instability for all G . For example, when $W = 100$ regions 1 and 2 have merged [Fig. 9(c)]. Increasing $|W|$ when $W < 0$ causes region 1 to eventually extend past region 2, despite region 2 continuing to move further to the right [see Fig. 9(c), $W = -200$], where the regions remain distinct to at least $W = -5000$. An example of the $m = 1$ mode eigenfunction for the left-hand unstable region in Fig. 9(d) is shown in Fig. 9(e), with all components showing a localized behavior at the interface, suggesting an interfacial mode caused by shearing from the rod, and a viscosity difference at the interface. The $m = 0$ modes have similar behavior. In Fig. 9(d) we observe a band of G where only $m = 1$ modes are unstable. Figure 9(f) shows the eigenfunction at the point $(k, G) = (0.1, 270)$ inside this region. Here, the real parts of w and v are at least a factor of 10^3 greater than the other parts of the eigenfunction.

When $W = 0$ and $\mu < 1$ we found that increasing μ pushed region 2 to the right, so that when $\mu = 0.9$ only region 1 was present up to at least $G = 10^4$. Figure 10 shows that the effect of switching the sign of W when $\mu = 0.9$ is similar to when $\mu = 0.5$. However, when $W = 50$ region 1 is completely stabilized, and total stabilization therefore occurs to at least $G = 10^4$. Although $W < 0$ initially destabilizes more modes in Fig. 10(a) (e.g., $W = -10$), $W = -50$ shifts region 1 to the right, so that there is stability when $G = 0$, a phenomenon not observed when $\mu = 0.5$. An eigenfunction, shown in Fig. 10(d), located in the shifted unstable region when $W = -50$, shows a heightened activity near the rod. At larger rod speeds more modes are rendered unstable,

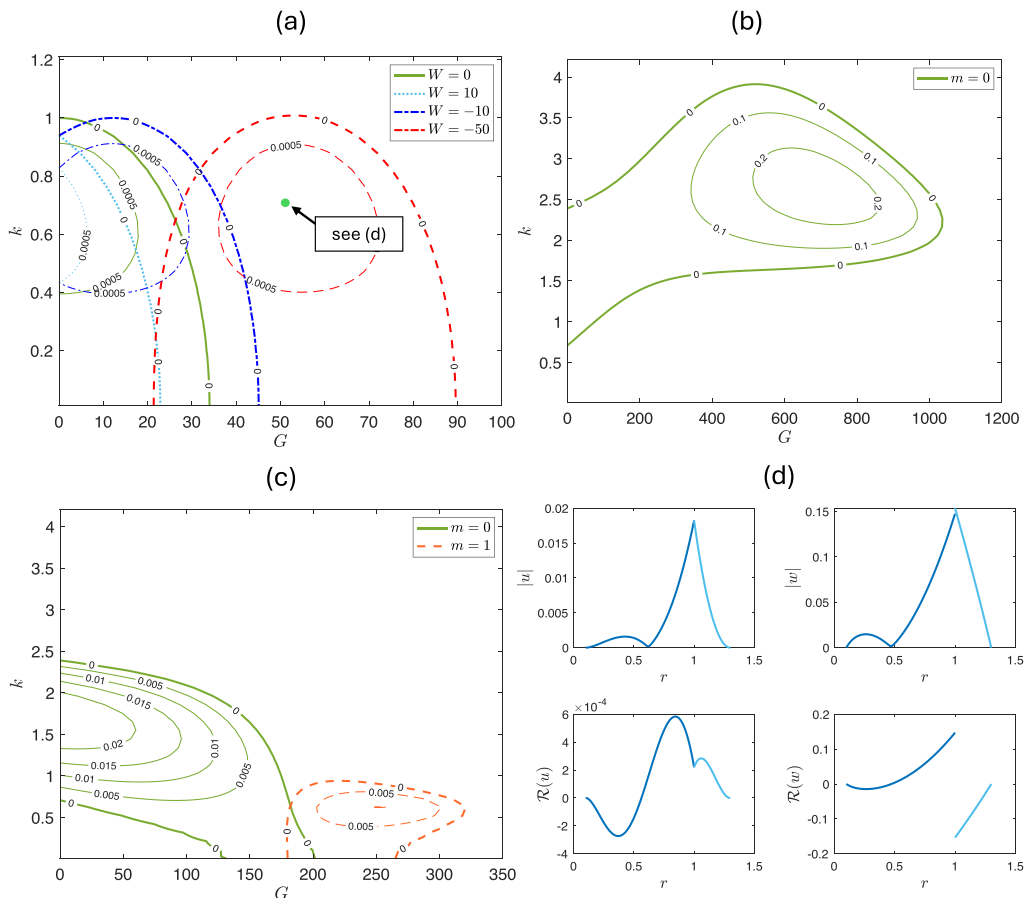


FIG. 10. Growth rates $s_r(G, k)$ for moving rod, $\mu = 0.9$, $R_0 = 0.1$, $R_2 = 1.3$, $J = 1$. Region 2 is absent up to at least $G = 10^4$ when $W = 0$. (a) $m = 0$ instability for region 1 as W varies. (b) $W = 150$, $\mu = 0.9$, and only $m = 0$ is unstable, but not for $k = 0$. (c) $W = -150$, $\mu = 0.9$, and both $m = 0, 1$ are unstable. For (a)–(c) the range of stable G extends up to at least $G = 10\,000$. For $W = -50$ the unstable region can be shifted to the right, for $W = 10$ the band of stable G is widened, and when $W = 50$ the system is stable for $G \leq 10\,000$. Past a critical value of $|W|$, modes are rendered unstable. (d) Eigenfunction when $\mu = 0.9$, $W = -50$, $G = 50$, $m = 0$, $k = 0.7$, and $s = 0.000859 - 1.066i$.

as shown when $W = 150$ [Fig. 10(b)] and $W = -150$ [Fig. 10(c)], with $m > 0$ modes important for $W = -150$. Further increase of $|W|$ renders $m \geq 0$ modes unstable irrespective of the sign of W .

We now examine the effect of moving the rod on region 3 in Fig. 11. Referring to Fig. 3(b), and keeping the same parameter values (here $J = 100$ and $\mu = 0.5$), we find that region 3 is shifted to the right when $W > 0$. If W is too large, then small G causes significant destabilization, as can be seen in Fig. 11(a) when $W = 1000$. Increasing W continues to shift region 3 to the right, and destabilizes low G . We observe that $G \leq 2.5 \times 10^4$ is unstable when $W = 5000$, despite pushing region 3 to $G > 2.5 \times 10^4$. In contrast, translating the rod in the opposite direction to the pressure-driven flow initially destabilizes $m = 1$ shear modes, so that region 3 expands to the left, as shown in Fig. 11(b) when $W = -1000$. Yet, past a critical $|W|$ the region is shifted to the right. For example, when $W = -5000$ in Fig. 11(c), we have a stable band of G .

Interestingly, the complete stabilizing influence of the rod's motion, seen in Fig. 10 when $\mu = 0.9$, is not observed if we increase the rod radius to $R_0 = 0.45$, or if we increase the outer-wall

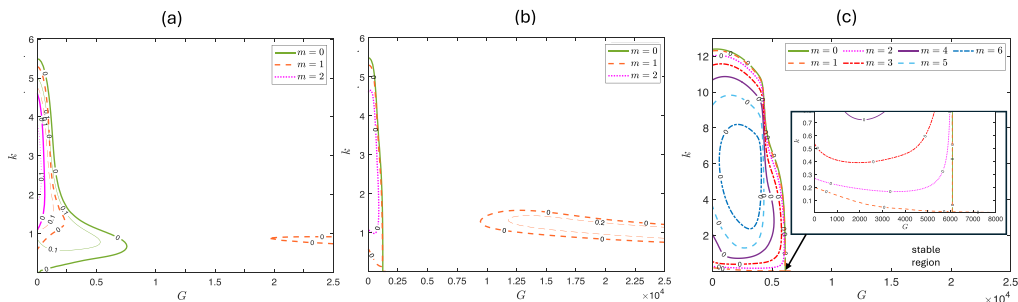


FIG. 11. Growth rates when $\mu = 0.5$, $R_2 = 1.3$, $R_0 = 0.1$, $J = 100$ and in (a) $W = 1000$, (b) $W = -1000$, and (c) $W = -5000$. Region 3 in Fig. 3(b) is shifted as W is varied.

radius to $R_2 = 2$, nor for the smaller viscosity ratio $\mu = 0.5$. In fact, when $\mu = 0.9$, translating the rod can produce stability when the pressure gradient is switched off, so that $G = 0$. In this case the sign of W is irrelevant. Figure 12(a) shows a stable region exists when $\mu = 0.9$ in this instance, and we find the left and right unstable regions merge when μ decreases, so that $\mu = 0.5$ is unstable for all W . Eigenfunctions for the left-side and right-side unstable regions are shown in Figs. 12(b) and 12(c), respectively. In Fig. 12(b) the eigenfunction is largest at the interface, but there is heightened activity near the rod in fluid 1, whereas in Fig. 12(c) the gradient is smooth in u and w is localized near the interface of the two fluids, suggestive of an instability due to interfacial effects.

We find that allowing the rod to translate can have a stabilizing effect on systems that are unstable for all G when $W = 0$. In the case when $\mu = 0.5$, $R_0 = 0.9$, $R_2 = 1.3$, and $J = 1$, Figure 13 shows that stabilization is possible over a range of G values for certain choices of $W \neq 0$ (the system is unstable for all G when $W = 0$). Typical eigenfunctions for $m = 0$ and $m = 1$ at a point in the leftmost unstable region of Fig. 13(a) are shown in Figs. 13(d) and 13(e) for $m = 0$ and $m = 1$, respectively, where u and w (and v for $m = 1$) are of comparable size, suggesting traveling waves. Upon comparing the eigenfunctions in Figs. 13(e) and 13(f), we see increasing the rod speed and pressure gradient produces more activity in the real part of v in fluid 1. The inviscid limit is achieved as either $G \rightarrow \infty$ and $W = O(1)$, $W \rightarrow \infty$ and $G = O(1)$, or both $W, G \rightarrow \infty$. Here, as G increases, and the parameters in Figs. 13(a)–13(c) are held fixed, and the flow profile becomes inviscidly unstable, as to be expected since the system is inviscidly unstable when $W = 0$ [see Fig. 5(c)].

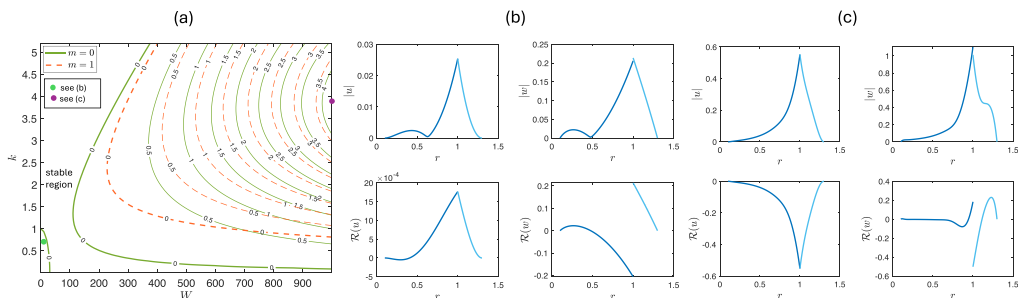


FIG. 12. (a) Growth rates $s_r(W, k)$ for $m = 0$ when $\mu = 0.9$, $R_0 = 0.1$, $R_2 = 1.3$, $J = 1$. Decreasing μ to $\mu = 0.5$ the unstable left and right regions merge. Eigenfunctions in left- and right-hand regions of (a) are given in (b) $W = 10$, $k = 0.7$, $J = 1$, $m = 0$, $G = 0$, $s = 0.0007234 - 0.7607i$ and (c) $W = 1000$, $J = 1$, $k = 3.9$, $m = 0$, $G = 0$, $s = 4.238 - 427.7i$, respectively.

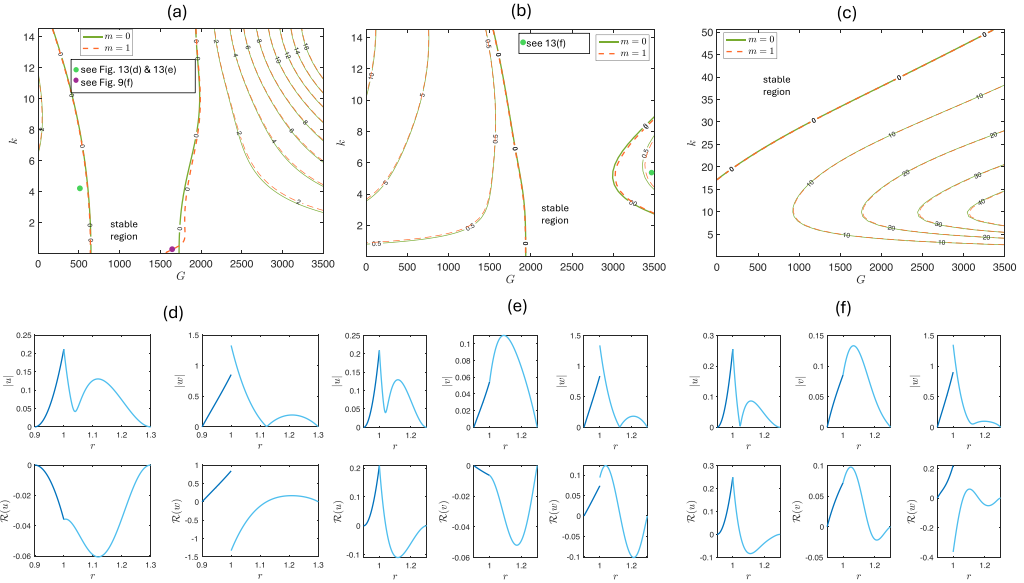


FIG. 13. Growth rates $s_r(G, k)$ for moving rod when $\mu = 0.5$, $R_0 = 0.9$, $R_2 = 1.3$, $J = 1$, $G = 0$. (a) $W = 50$, (b) $W = 150$, and (c) $W = -50$. The eigenfunctions for the left-hand region of (a) are given in (d) for $W = 50$, $G = 500$, $k = 5.2$, $m = 0$, $s = 0.1726 - 261.9i$, and (e) for $W = 50$, $G = 500$, $k = 5.2$, $m = 1$, $s = 0.1642 - 261.95i$. The eigenfunction for the $m = 1$ unstable region on the right-hand region of (a) resembles Fig. 9(f). (f) The eigenfunction for the right-hand region of (b) when $m = 1$, $k = 6$, $G = 3500$, $W = 150$, $s = 0.72 - 1152i$. Stable regions exist for $0 < W < 150$ at least. Large $W < 0$ is unstable for all G . The flow is inviscidly unstable in each case.

Next we consider the effect of enlarging the annular gap by increasing the outer-wall radius from $R_2 = 1.3$ up to $R_2 = 2$. The results are shown in Fig. 14. As for Fig. 13 the effect of increasing W is to shift the stable G window to the right. Increasing J is found to narrow the stable G window. The eigenfunctions for the leftmost and rightmost unstable regions of Figs. 14(a) and 14(b) resemble

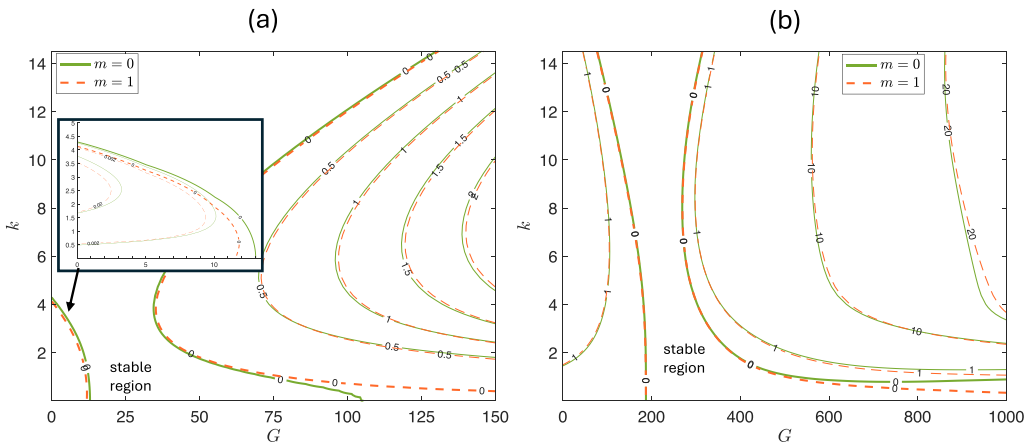


FIG. 14. Growth rates $s_r(G, k)$ when $\mu = 0.5$, $R_0 = 0.9$, $R_2 = 2$, $J = 1$. (a) $W = 10$ and (b) $W = 150$. The stable G band shifts to the right as W is increased.

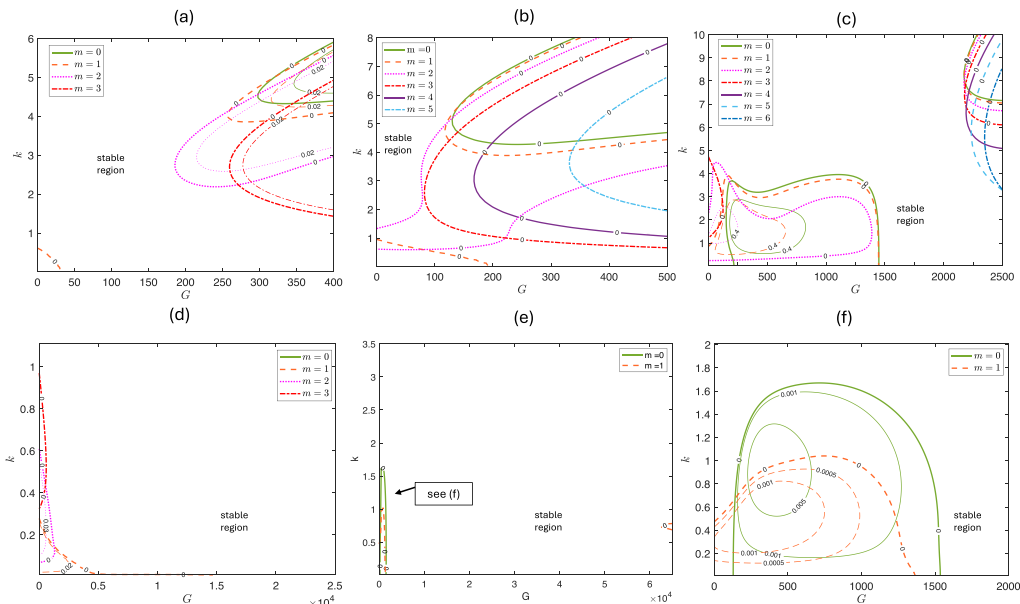


FIG. 15. Growth rates plotted when $\mu = 1.5$, $R_2 = 2.0$, $R_0 = 0.45$. (a) $W = -10$, $J = 1$, (b) $W = -50$, $J = 1$, (c) $W = 100$, $J = 1$, (d) $W = -5000$, $J = 100$ (stability to at least $G = 6.5 \times 10^4$), (e) $W = 100$, $J = 100$, and (f) an enlarged image of (e) at small G . Varying J and W shifts the unstable regions that exist when $W = 0$ in Fig. 7.

those shown in Figs. 13(d)–13(f) when the unstable modes are close to the stable region. If G is increased so as to move away from the stable region, the eigenfunction becomes increasingly localized at the interface, as expected.

Finally, in most cases considered when $G \neq 0$, $W < 0$ renders modes unstable, and $W > 0$ is favorable for stabilizing modes. However, clearly region 2 is a caveat to this, as well as the existing examples where $W < 0$ would stabilize a given G , whereas $W > 0$ would not.

2. $\mu > 1$: More viscous outer fluid

When $\mu > 1$ and the outer fluid is the more viscous, switching the sign of the rod velocity has the opposite effect on region 1 and region 2 modes to that seen for $\mu < 1$. However, region 3 is shifted in the same manner for $W \neq 0$ when $\mu < 1$ and $\mu > 1$. This is seen upon comparing Fig. 7 when $W = 0$ and Fig. 15 where $W \neq 0$. In Fig. 15(a) $W = -10$, and region 2 has grown to the left. Although $m = 0$ in region 1 has been stabilized, $m = 1$ modes are destabilized at small G . Increasing $|W|$ to $W = -50$ in Fig. 15(b) causes regions 1 and 2 to merge, and all G are unstable. Conversely, $W > 0$ shifts $m = 0$ region 1 modes to the right, but also destabilizes $m > 0$ modes for small G [see Fig. 15(c)]. Region 2 modes are shifted to the right, allowing for a range of stable G that were unstable when $W = 0$ (cf. Figs. 7 ($W = 0$) and 15(c) ($W = 100$)). As W is increased further, the stable region between regions 1 and 2 is continuously shifted to the right, and this is observed for $W > 0$ to at least $W = 1000$. When $J = 100$ and $W = 0$ we have stability between region 1 and region 3 in Fig. 7. When $W < 0$, small $|W|$ pushes region 3 to the left, destabilizing modes. But, past a critical value, region 3 is stabilized and when $W = -5000$ in Fig. 15(d), region 3 has disappeared for $G \leq 6.5 \times 10^4$. What's more, $m = 0$ modes in region 1 are stabilized, but $m > 0$ are unstable for sufficiently small G . Increasing $W > 0$ immediately shifts region 3 to the right. Yet, $m \geq 0$ modes are rendered unstable at lower G [see Figs. 15(e) and 15(f), where $W = 100$, $J = 100$]. Upon comparing Figs. 15(c) and 15(f) we see that increasing J has stabilized $m > 1$ modes, but the

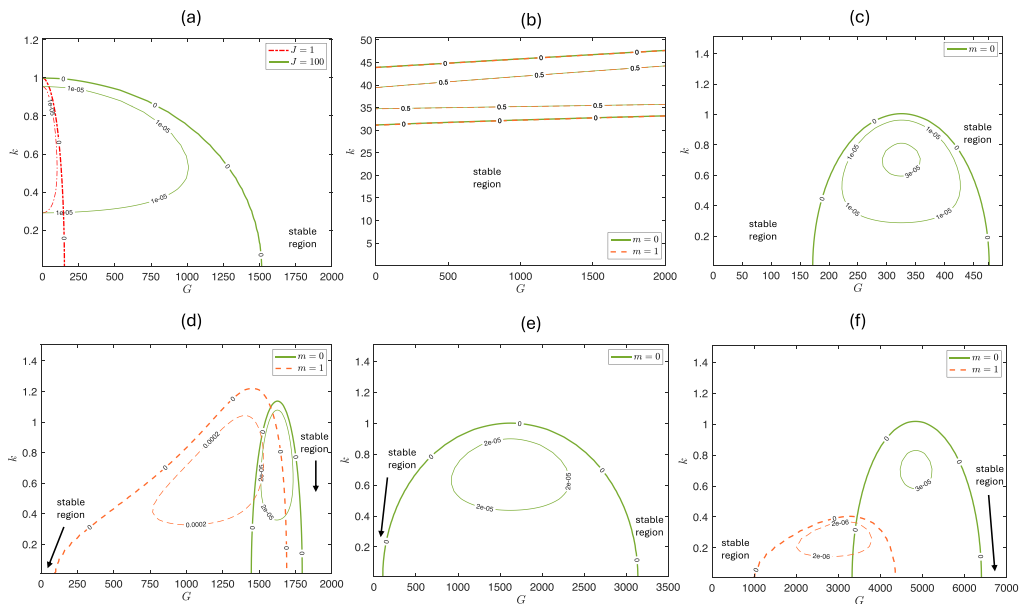


FIG. 16. Growth rates $s_r(G, k)$ for $\mu = 1.2$, $R_0 = 0.9$, $R_2 = 1.3$. (a) $m = 0$, $W = 0$, $J = 1, 100$, and there is stability up to at least $G = 10\,000$; (b) $J = 1$, $W = -1000$; (c) $J = 1$, $W = 10$; (d) $J = 1$, $W = 50$; (e) $J = 100$, $W = 50$; (f) $J = 100$, $W = 150$. In panels (c)–(f) there is stability up to at least $G = 10\,000$. Varying $W > 0$ and J shifts the regions of instability. Moreover, there is complete stabilization for the range $G \leq 10\,000$ when W ranges from -10 down to at least -400 and $J = 1, 100$.

range of unstable G is increased slightly. Thus, large G favors large $|W|$ for stability, but small G will likely be unstable.

Complete stabilization of region 1 is possible when $\mu > 1$ and $W < 0$, in contrast to $\mu < 1$ which required $W > 0$ (see Fig. 10). This is observed when R_2 is reduced, and R_0 is increased to give $R_2 = 1.3$, $R_0 = 0.9$. Consequently, if region 2 does not exist for $G < G_R$, we find complete stability for $0 \leq G \leq G_R$ for a critical range of $W < 0$ that depends on the other parameters. For a stationary rod, increasing J or decreasing $\mu > 1$ caused region 2 to shift to the right. We find $0 \leq G \leq 10^4$ is stable when $J = 100$, $\mu = 1.5$ and W ranges from $W \leq -50$ to at least $W = -150$. Alternatively, decreasing μ to $\mu = 1.2$ pushed region 2 to $G > 10^4$ when $J = 1$. Region 1 for $J = 1, 100$ when $\mu = 1.2$ is shown in Fig. 16(a), and complete stabilization occurs for $J \geq 1$, $0 \leq G \leq 10^4$, and $W \leq -10$. However, $W < 0$ shifts region 2 to the left, and region 2 appears for $G \leq 10^4$ when $W = -500$, $J = 1$. Maintaining $J = 1$ and increasing $|W|$ results in region 2 expanding further to the left, and when $W = -1000$, $J = 1$ in Fig. 16(b) it joins with the y axis and all G are unstable. Nevertheless, increasing J stabilizes this region, so that when $J = 100$ there is complete stability for $0 \leq G \leq 10\,000$ when $-1000 \leq W \leq -10$.

Moreover, for these same values of $R_2 = 1.3$, $R_0 = 0.9$, moving the rod in the same direction as the driving pressure gradient translates region 1 to the right, away from $G = 0$, so that $0 \leq G \leq G_L$ is stable. This is markedly illustrated by the case when $\mu = 1.2$, but also observed when $\mu = 1.5$. The remaining panels in Fig. 16 show the effect of translating the rod in the same direction as the driving pressure gradient. At $W = 10$ [Fig. 16(c)] the instability remains axisymmetric but now spans a window of G values away from zero. The window boundaries are accurately predicted by the long-wave analysis in Sec. III C. When $W = 50$ the first nonaxisymmetric mode, $m = 1$, is destabilized [Fig. 16(d)] and increasing W renders more modes unstable. Figures 16(e) and 16(f) show the effect of increasing J and hence the capillary force at the interface. Comparing Figs. 16(d) and 16(e), we see that increasing J has stabilized $m = 1$ modes, but in destabilized ($c \rightarrow b$) $m = 0$

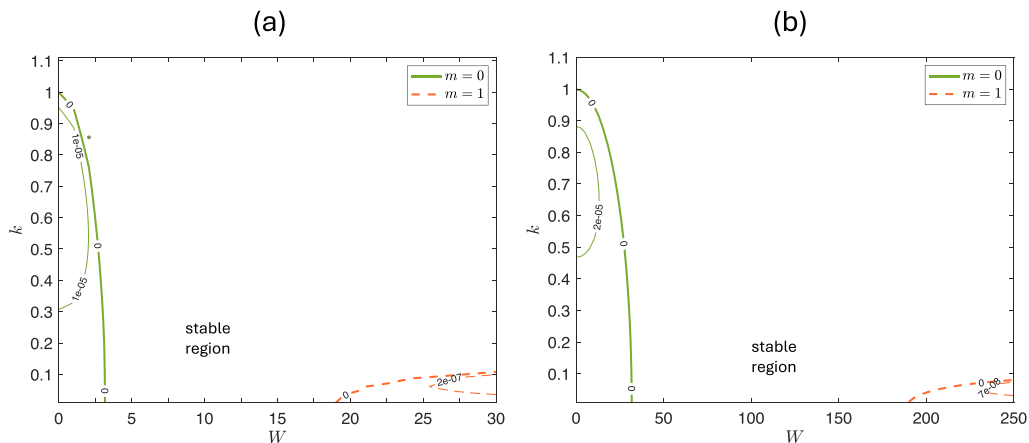


FIG. 17. Growth rates $s_r(W, k)$ when $\mu = 1.5$, $R_0 = 0.9$, $R_2 = 1.3$, $G = 0$: (a) $J = 1$ and (b) $J = 100$.

modes. Increasing W from $W = 50$ in Fig. 16(e), to $W = 150$ in Fig. 16(f), destabilizes $m = 1$ modes, but also produces a stability window over $0 \leq G < 1000$.

In the absence of a pressure gradient, Fig. 17 shows the effect of the rod translation when $\mu = 1.5$. In this case it is possible for the only unstable modes to be nonaxisymmetric. Increasing J from $J = 1$ to $J = 100$ extends the stable W range, although at relatively low W , $J = 1$ is favorable. This suggests that the leftmost region is a capillary instability, whereas the rightmost region is an outcome of shearing from the translation of the rod that can be dampened by increasing J . We find decreasing μ increases the band of stable W values too.

When $W = 0$, increasing the outer-wall radius to $R_2 = 2.0$ resulted in an unstable configuration (see Fig. 8), but a stable range of G can be achieved by translating the rod. We observe that increasing $|W|$ with $W < 0$ stabilizes $m = 0$ in the lower unstable region of Fig. 8, but $m > 0$ remain unstable at small k . However, $W > 0$ can produce a band of stable G , $G_L \leq G \leq G_R$. The lower unstable region is shifted to the right as W increases, but a new region of unstable $m = 1$ modes is produced for $G < G_L$. This is shown when $W = 100$ in Fig. 18, where in Fig. 18(a) $J = 1$ and in Fig. 18(b) $J = 100$. Comparing Figs. 8(a) and 18(a), we observe region 2 is shifted to the right by the increase in W , as expected, and $m > 2$ modes are destabilized in the right-hand lower unstable region. If W is too large, a new region of unstable short waves emerges when $J = 1$ [see Fig. 18(c), $W = 500$]. An eigenfunction for the region [see Fig. 18(d)] shows a localized behavior near the interface, suggesting that when the shear from the rod is strong enough, and the inner fluid sufficiently thin, a short-wave interfacial instability occurs. Indeed, upon increasing capillary forcing at the interface, this region is stabilized.

For a stationary rod, the case when $\mu = 1.5$ and $R_0 = 0.1$ (and various R_2, J) was seen to be unstable for all G in Fig. 6. A window of stability can be created by translating the rod such that $W < 0$. This is shown in Fig. 19 for the pairs $(R_2, J) = (1.3, 1)$ and $(2, 1)$; compare Figs. 6(a) and 6(c) for a stationary rod. The eigenfunctions for the left and right regions in Figs. 19(a) and 19(b), and the right unstable regions in Figs. 19(c) and 19(d), behave similarly to the left and right eigenfunctions in Fig. 13. The corresponding eigenfunctions for the left-most unstable region in Figs. 19(c) and 19(d), consisting of $m = 1$ modes, have notably more activity in fluid 1, and an example is shown in Fig. 19(e). Those in Fig. 19(f), related to the upper island of shorter wave instabilities in Fig. 19(d), are localized around the interface. As $|W|$ increases, we observe the island expanding to the left, and it eventually reaches $G = 0$, suggesting an interfacial instability caused by the shearing of the rod coupled with the base flow. When $R_2 = 2.0$, increasing $|W|$ and J shifts the stable region to different values of G , and a sufficiently large J stabilizes the upper unstable island. For $R_2 = 1.3$, as $|W|$ increases, the stable window is shifted to the right until, at a critical W , the

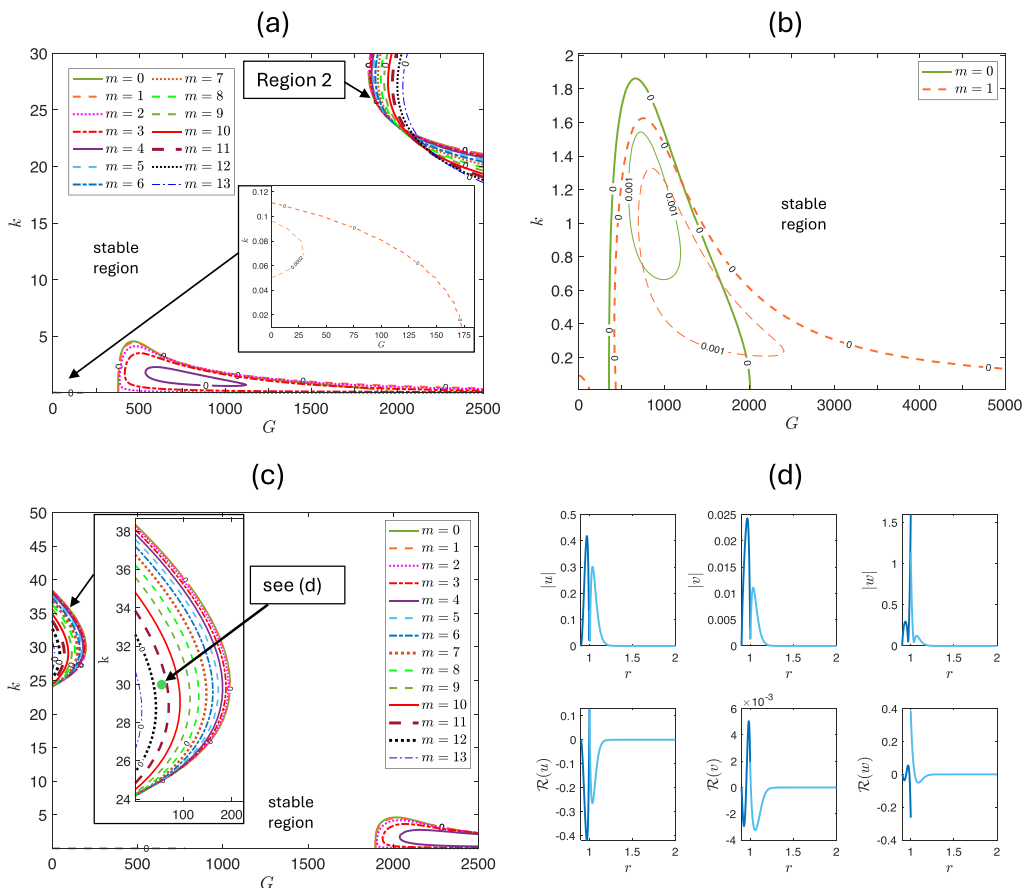


FIG. 18. Growth rates $s_r(G, k)$ for $\mu = 1.5$, $R_0 = 0.9$, and $R_2 = 2.0$. (a) $W = 100, J = 1$ and (b) $W = 100, J = 100$. (c) $W = 500, J = 1$, and a new region of instability exists, where (d) an eigenfunction is shown for the region when $m = 1, k = 30, G = 50, W = 500, s = 0.988 - 12310.4i$. Increasing J dampens the instability caused by the moving rod.

$m = 0$ neutral curves that border the stability window collide and the system becomes unstable for all G . Moreover, we find increasing J is undesirable when $R_2 = 1.3$, and is more unstable than $J = 1$. Similarly, increasing R_0 to $R_0 = 0.45$ when $R_2 = 1.3$ destabilized the system, and we observed no stability for $W = 0$ or a translation of the rod. This suggests a suitable ratio of fluid thicknesses is required for stability when $\mu > 1$.

Finally, for $\mu > 1$ the preferable sign of W for stability depends on the desired G , although in general we found $W < 0$ tends to produce more of a stabilizing effect than taking $W > 0$. However, exceptions to this include region 2, which is destabilized to lower G by $W < 0$, and the parameters in Fig. 18 which required $W > 0$ for stable values of G .

V. CONCLUDING REMARKS

We have studied the stability of rod annular flow (RAF) of two concentrically arranged viscous fluids moving through a cylindrical pipe with a solid rod mounted along its axis. The flow is driven by an axial pressure gradient and/or the translation of the rod along its axis at constant speed. Investigating the stability of this configuration is a complex problem which depends on eight independent parameters ($\mu, G, J, R_0, R_2, W, k, m$). It is therefore impractical to establish the

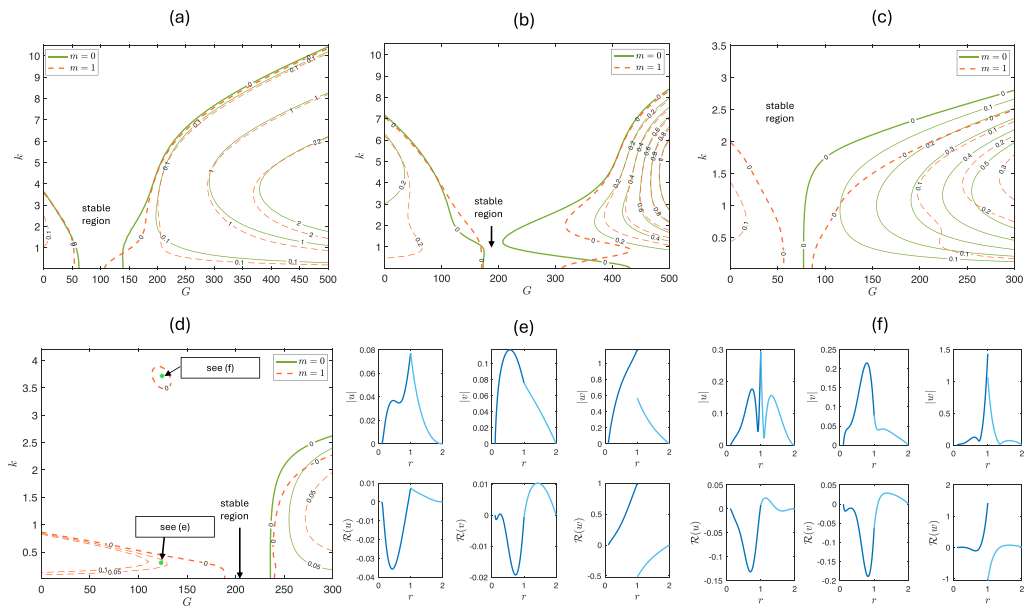


FIG. 19. Growth rates $s_r(G, k)$ when $\mu = 1.5$, $R_0 = 0.1$, and $J = 1$. (a) $W = -50$, $R_2 = 1.3$, (b) $W = -150$, $R_2 = 1.3$, and once $W = -250$ the unstable regions have merged. (c) $W = -50$, $R_2 = 2.0$, (d) $W = -150$, $R_2 = 2.0$. Increasing $|W|$ shifts the stable region to the right, and past a critical value the system is unstable for all G . (d) Eigenfunctions corresponding to the $m = 1$ unstable regions, where (e) $R_2 = 2$, $W = -150$, $G = 125$, $k = 0.3$ and $m = 1$, $s = 0.061 - 6.13i$, and (f) $R_2 = 2$, $W = -150$, $G = 125$, $k = 3.7$ and $m = 1$, $s = 0.0036 - 79.70i$, corresponding to the upper circle region. The left and right regions in (a) and (b) behave similarly to the eigenfunctions in Fig. 13.

optimal arrangement for stability, whichever fluid is the more viscous. The stability behavior is quite sensitive to the geometry, but some comments on the general trends can be made. The axisymmetric capillary instability can in some circumstances be controlled by the flow but, equally, the system may be unstable to all axisymmetric long waves for any base-flow strength. Furthermore, the flow may be prone to instabilities of various types. In broad terms, the group we categorize as “region 2” can have $m \geq 0$ and fairly large k . Stronger surface tension can control these at least partially. The “region 3” modes do not feel surface tension greatly, as their eigenfunctions are localized away from the interface itself, and they appear to be connected with the shear modes described by Refs. [17,18,21]. The unstable k values appear to approach zero as G increases. In contrast, there is also a class of flows for which the gradient change at $r = 1$ is contrary to the general profile shape, which are inviscidly unstable. Such flows are often unstable for all values of G when the rod is stationary.

For a stationary rod, if the inner fluid is more viscous, $\mu < 1$, the flow is unstable when the rod radius exceeds a threshold value or when the outer fluid is too thick. Conversely, if the outer fluid is the more viscous, $\mu > 1$, but not too thick, then the rod radius must be sufficiently large to achieve stability. In both cases, if the parameter set is such that there exists a band of stable G values, between “regions 1 and 2,” then this band is widened by increasing the capillary parameter J . Otherwise, if such a G band does not exist, then raising J can stabilize short waves, but the system will remain unstable. Moreover, for critical ranges of R_2, R_0, μ , a sufficiently strong pressure gradient destabilizes nonaxisymmetric modes, while axisymmetric modes remain stable if J is sufficiently large. Thus, for a strong pressure gradient, that is a large value of G , nonaxisymmetric modes are important and should not be neglected. This is in line with what has been found in previous works [1,17,19,21].

The system is even more complex when the rod is moving. The stabilizing influence of W depends greatly on the direction of the translation and μ , where $W > 0$ moves in the same direction as the pressure-driven flow, and $W < 0$ moves counter to the driven flow. In general, longer-wave instabilities seem to be dampened by $W > 0$ when $\mu < 1$, but short waves, like region 2 modes, are destabilized when $W > 0$. When $\mu > 1$, the converse is true. However, region 3 with $W \neq 0$ behaves the same irrespective of $\mu > 1$ or $\mu < 1$, consolidating the theory that it is not an interfacial mode. Physically, W moving in the direction of the pressure-driven flow effectively reduces the friction at the inner boundary. However, $W < 0$ creates a larger friction at the inner boundary for small $|W|$. When $W < 0$ is large enough, it counteracts the pressure-driven flow, and a larger G is required for region 3 modes. Generally, a strong enough J will still dampen short waves, but $m = 0$ long waves seem more susceptible to capillary instabilities when the rod is moving than when it is stationary.

A stable configuration can be identified upon moving the rod, for rod radii that were unstable when the rod is stationary. For $\mu < 1$, this occurs when the rod radius is large and the outer fluid thicker than the inner fluid, where $W > 0$ produces new stability regions in parameter space. When the rod radius is small, and the inner fluid is thicker than the outer fluid, and $W > 0$ can produce stability for a much larger range of G than when $W = 0$, including $G = 0$. However, this seems to happen when the viscosity ratio μ is close to unity. Similarly, when $\mu > 1$, a thick rod is no longer required once $W \neq 0$. If the inner fluid is comparably thicker than the outer fluid, $W < 0$ is required, whereas $W > 0$ is required if the outer fluid is a lot thicker. Moreover, if a range of stable G existed when $W = 0$, and the outer fluid is thicker with $\mu > 1$, $W < 0$ can produce stability for a larger range of G than when the rod was stationary. If $G = 0$ then complete stabilization can occur, with a larger range of stable W when μ is just above unity. Taking J larger seems to have a destabilizing effect in most cases for $G \neq 0$, suggesting the system is more susceptible to an inertial instability when the rod is moving, than when it is stationary.

There appears to be a small range of rod velocities that will produce stabilizing effects for the parameter values considered, in contrast to a one-fluid Couette-Poiseuille flow, where a sufficiently large rod velocity $W > 0$ can always stabilize the system [1,20]. We have found that for both a stationary and a moving rod, the relative sizes of the rod radius and the fluid thicknesses are of great importance for stability, and this is in keeping with what has been seen in the literature on RAF and CAF.

In conclusion, these findings hold significant importance for practical applications and future experimental work. In particular, they demonstrate that with the introduction of a central rod, a two-fluid CAF can be sustained, even when the outer fluid is more viscous than the inner fluid. In contrast, without the rod, the fluid with higher viscosity will inevitably occupy the center [13]. Nevertheless, the limitations of a linear analysis should be remembered. Even the stable states may be prone to subcritical bifurcations at higher Reynolds numbers. Future work could involve a weakly nonlinear analysis of the problem to provide further insight into the instability when either the inner fluid or the outer fluid is thin. Allowing the rod to rotate would also be of interest, but likely would be destabilizing. Driving an electric current along the rod to create an azimuthal magnetic field leads to further possibilities of interest in magnetohydrodynamics and ferrohydrodynamics. In the latter case, the work of Ref. [26] suggests that by allowing one of the two fluids to be a ferrofluid, which interacts with the magnetic field, the stability of the system can be controlled further. These extensions are the subject of ongoing investigations.

-
- [1] A. G. Walton, The linear and nonlinear stability of thread-annular flow, *Philos. Trans. R. Soc. A* **363**, 1223 (2005).
 - [2] L. Preziosi and F. Rosso, Interfacial stability in a two-layer shearing flow between sliding pipes, *Eur. J. Mech. B: Fluids* **10**, 269 (1991).
 - [3] L. Rayleigh, On the capillary phenomena of Jets, *Proc. R. Soc. London* **29**, 71 (1879).

- [4] Tomotika, On the instability of a cylindrical thread of a viscous liquid surrounded by another viscous fluid, *Proc. R. Soc. London, Ser. A* **150**, 322 (1935).
- [5] R. M. Christiansen and A. N. Hixson, Breakup of a liquid in a denser liquid, *Ind. Eng. Chem.* **49**, 1017 (1957).
- [6] B. J. Meister and G. F. Scheele, Drop formation from cylindrical jets in immiscible liquid systems, *AIChE J.* **15**, 700 (1969).
- [7] S. L. Goren, The instability of an annular thread of fluid, *J. Fluid Mech.* **12**, 309 (1962).
- [8] E. J. Hinch, A note on the mechanism of the instability at the interface between two shearing fluids, *J. Fluid Mech.* **144**, 463 (1984).
- [9] D. D. Joseph, M. Renardy, and Y. Renardy, Instability of the flow of two immiscible liquids with different viscosities in a pipe, *J. Fluid Mech.* **141**, 309 (1984).
- [10] D. D. Joseph, G. S. Beavers, and G. S. Beavers, Non-uniqueness and stability of the configuration of flow of immiscible fluids with different viscosities, *J. Fluid Mech.* **141**, 319 (1984).
- [11] C.-S. Yih, Instability due to viscosity stratification, *J. Fluid Mech.* **27**, 337 (1967).
- [12] A. P. Hooper and W. G. C. Boyd, Shear-flow instability at the interface between two viscous fluids, *J. Fluid Mech.* **128**, 507 (1983).
- [13] P. J. Redberger and M. E. Charles, Axial laminar flow in a circular pipe containing a fixed eccentric core, *Can. J. Chem. Eng.* **40**, 148 (1962).
- [14] L. Preziosi, K. Chen, and D. D. Joseph, Lubricated pipelining: Stability of core-annular flow, *J. Fluid Mech.* **201**, 323 (1989).
- [15] H. H. Hu and D. D. Joseph, Lubricated pipelining: Stability of core-annular flow. Part 2, *J. Fluid Mech.* **205**, 359 (1989).
- [16] P. A. M. Boomkamp and R. H. M. Miesen, Nonaxisymmetric waves in core-annular flow with a small viscosity ratio, *Phys. Fluids* **4**, 1627 (1992).
- [17] H. A. Dijkstra, The coupling of interfacial instabilities and the stabilization of two-layer annular flows, *Phys. Fluids* **4**, 1915 (1992).
- [18] A. P. Hooper, The stability of two superposed viscous fluids in a channel, *Phys. Fluids* **1**, 1133 (1989).
- [19] M. J. Russo and P. H. Steen, Shear stabilization of the capillary breakup of a cylindrical interface, *Phys. Fluids* **1**, 1926 (1989).
- [20] A. W. H. Wong and A. G. Walton, Axisymmetric travelling waves in annular Couette–Poiseuille flow, *Q. J. Mech. Appl. Math.* **65**, 293 (2012).
- [21] C. J. Heaton, Linear instability of annular Poiseuille flow, *J. Fluid Mech.* **610**, 391 (2008).
- [22] A. P. Bassom, M. G. Blyth, and D. T. Papageorgiou, Using surfactants to stabilize two-phase pipe flows of core–annular type, *J. Fluid Mech.* **704**, 333 (2012).
- [23] M. G. Blyth and A. P. Bassom, Stability of surfactant-laden core–annular flow and rod–annular flow to non-axisymmetric modes, *J. Fluid Mech.* **716**, R13 (2013).
- [24] S. Chandrasekhar, *Hydrodynamic and Hydromagnetic Stability*, Dover Books on Physics Series (Dover Publications, New York, 1981).
- [25] P. G. Drazin and W. H. Reid, *Hydrodynamic Stability*, 2nd ed., Cambridge Mathematical Library (Cambridge University Press, Cambridge, UK, 2004).
- [26] S. H. Ferguson Briggs and A. J. Mestel, Linear stability of a ferrofluid centred around a current-carrying wire, *J. Fluid Mech.* **942**, A20 (2022).